ANALYSIS AND MODELING OF A MICRO VARIABLE CAPACITANCE ELECTROMECHANICAL ENERGY CONVERTER

by

AMITA JINDAL

Presented to the Faculty of the Graduate School of

The University of Texas at Arlington in Partial Fulfillment

of the Requirements

for the Degree of

MASTER OF SCIENCE IN ELECTRICAL ENGINEERING

THE UNIVERSITY OF TEXAS AT ARLINGTON

December 2005

Copyright © by Amita Jindal

All Rights Reserved

ACKNOWLEDGEMENTS

I would like to express my sincere gratitude to my advisor, Dr. Babak Fahimi, for his patience and invaluable guidance provided throughout the conceptualization and writing of this thesis.

I would like to thank my committee members, Dr. Wei-Jen Lee and Dr Jung-Chih Chiao, for their valuable support and assistance.

Also, I express my heartfelt gratitude to my Family and Friends for being a constant source of moral support, love and inspiration for me.

August 11, 2005

ABSTRACT

ANALYSIS AND MODELING OF A MICRO VARIABLE CAPACITANCE ELECTROMECHANICAL ENERGY CONVERTER

Publication No. _____

Amita Jindal, MS

The University of Texas at Arlington, 2005

Supervising Professor: Dr. Babak Fahimi

Research and development in microelectromechanical systems (MEMS) have made remarkable progress since late 80's. Micro-machines are an integral part of MEMS. However, these machines are not often discussed in most electric machines, power electronics and drive forums due to the relative newness of these machines.

This thesis provides an in-depth analysis of a variable capacitance micro-machine (VCM). It gives an insight into the effects of machine geometry, on capacitance and torque profiles of the machine. Tangential and radial components of the electrostatic forces in the air gap of the machine have been investigated to explore the effects of mutual flux. These studies have been performed using the finite element model of an 8/6, four phase micro VCM. Furthermore, the analytical modeling of the

phase capacitance of the machine has been discussed. Also, dynamic model of the machine has been developed in SIMULINK, to maximize torque/ volt of the machine.

TABLE OF CONTENTS

LIST OF ILLUSTRATIONS

LIST OF TABLES

CHAPTER 1

INTRODUCTION

1.1 Background

Some hundred years of design and analysis of electric machinery has been accomplished by those specializing in power systems, machinery, power electronics, and motor drives [1]. In the last decade, the technology of micromachining has emerged as a method to create very small sensors and actuators for use in electromechanical systems. Electric micro-machines are an integral part of this emerging technology [2].

The advantages of micro machines over their macro-sized counterparts are manifold. These machines typically lead to higher safety due to their small size, have better cost efficiency and smaller modular size that leads to more options in usage. In addition, higher surface to volume ratio helps to build a more compact system that can be easily integrated with the electronics required for the closed loop control [3].

Micro motors are currently not being widely used in industrial applications, but are in developmental stage that suggests a near-future explosion of applications. Biomedical applications such as drug delivery systems, surgical tools and probes are considered very promising [4]. The envisioned applications for micro-machines, designed for high speed and torque, include dime-sized gas turbine generators powering mobile electronic devices, motor–driven pumps and compressors for handheld analytical instruments, or micro coolers for electronics, sensors and people.

Micro machines could be linear or rotary. The main advantage of rotary electric machines is that it has one axis with unlimited motion. Although rotary micro-motors can be implemented with both electrostatic as well as magnetic design, electrostatic actuation is considered to be more practical, both for theoretical and implementation reasons [5]. This is due to the fact that as the dimensions of the machine become smaller, electrostatic forces scale advantageously when compared to magnetic forces that dominate at the dimension starting from millimeter range. Therefore, in addition to being more convenient to build in small scales, electrostatic motors have fundamentally superior force producing properties.

Electrostatic rotary micro-motors can exist in various forms and types. These can be classified depending upon their functional qualities as follows:

1) Variable Capacitance Micro-motors

2) Electrostatic Induction Micro-motors

3) Wobble Micro-motors

Amongst all these, Variable Capacitance Micro-motor has the simplest mechanical structure and is simply based upon a modified parallel plate capacitance model. Much research recently has been performed to improve understanding the design rules and optimization process of rotary electrostatic variable capacitance micro-motor in particular [6].

This thesis provides an insight into the variable capacitance micro-motor based on a modified parallel plate capacitance model and is organized into a short introduction, a section dealing with an overview of electrostatic machines, a section

dealing with the fundamentals of micro variable capacitance machine (VCM), a section dealing with the finite element analysis (FEA) of the micro VCM geometry followed by a section describing the modeling of phase capacitance of the micro VCM using different modeling approaches, a section presenting the dynamic model of the micro VCM developed using Simulink and torque/volt maximization of the micro VCM operating at different speeds, and conclusions.

1.2 Motivation and Objective

Micro machines can be defined as very small devices in the millimeter and sub-millimeter range. These can provide unrestrained motion in at least one degree of freedom. These machines are not often discussed in most electric machines, power electronics and drive forums. This is due to the relative newness of the devices and that they are constructed with semiconductor processing techniques. As such, drive systems operation and design, as well as in depth investigation of various fundamental and basic issues is generally neglected [5]. Although the functional requirements needed to be met by a micro electric machine is the same as that of a conventional macro machine, the operational performance involving electromechanical, magnetic and electrostatic characteristics of micro-machines vary significantly from that of conventional machines. For a clear comprehension of the complexities involved in the micro-machine operating environment, analysis and optimization of the actuation mechanism, various fields, forces and other time varying physical quantities is required.

Switched reluctance motors (SRM), due to their very simple mechanical structure and large force generation capability, preserve competence in the miniaturized

world for micro electro mechanical systems applications. In fact variable capacitance motors (VCM) represent the electric dual configuration for SRM. Applications of micro VCM include micro positioning stage, micro fluidic devices, minimally invasive surgery, relays and switches [7].

In this thesis, a two dimensional finite element model of a micro VCM will be developed using Maxwell Electrostatic Solver. Effects of the machine geometry on capacitance profile and torque generating capability of the machine will be studied. Capacitance and torque profiles will be extracted from the FEA and their analytical modeling will be done using three different modeling approaches. Then, results of the three approaches will be compared. Finally, dynamic model of the micro VCM along with its drive electronics will be developed using Simulink to maximize the torque/volt performance of the micro VCM by optimizing the conduction angles of the drive electronics.

CHAPTER 2

OVERVIEW OF ELECTROSTATIC MICROMACHINES

Making machines as small as insects has been dreamed of by scientists for many years. Such machines called micro electromechanical systems (MEMS) in the United States and micro-machines in Japan are micro-miniature systems composed of mechanical devices with electrical devices [8]. These have been an active area of research for commercial and military applications**.** Although electrostatic as well as magnetic actuation methods can be used for micro-machines, electrostatic micro-motors are advantageous when compared to the magnetic micro-motors because of the favorable and impressive scaling of various electromechanical quantities like the electrostatic force, power and energy from the macro domain to the micro domain. Also, electrostatic micro-motors are relatively easy to fabricate, have simple material requirements and manufacturing compatibility with micro-fabrication technologies. The figure 2.1 shows the cross-sectional view of a typical electrostatic micro-motor.

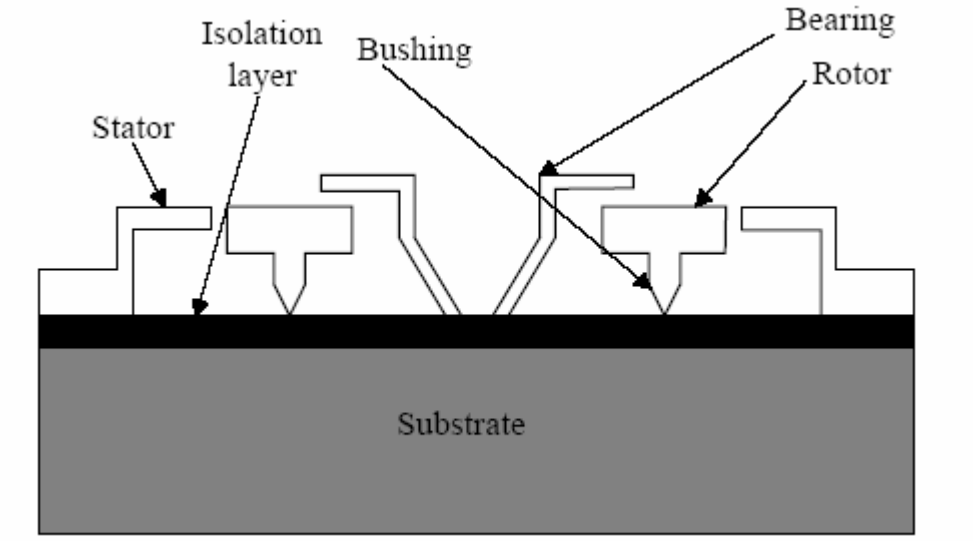

Figure 2.1 Cross Section of a typical electrostatic micro-motor [9]

2.1 Classification of Electrostatic Micro-motors

Electrostatic micro-motors can exist in various different forms and types. Depending upon their principle of operation, these can be classified as follows:

1) Variable Capacitance Micro-motors

2) Electrostatic Induction Micro-motors

3) Wobble Micro-motors

1) Variable Capacitance Micro-motors: A variable capacitance micro-motor is conceptually the simplest rotary micro-motor as it has very simple mechanical structure. Its construction requires only good insulators and simple open loop pulses are sufficient for its excitation. It is a synchronous machine that produces a steady state drive torque output at synchronously rotating speed of the stator field. The rotor is grounded to zero and stator electrodes are excited. As the voltage is applied to the stator electrodes, electrostatic field develops between the stator and the rotor that gives rise to

electrostatic forces tending to align the rotor poles with the excited stator electrodes. Its principle of operation is based on a simple parallel plate capacitor arrangement. The torque produced in the machine depends upon the rate of change of energy stored in variable stator-rotor capacitance with respect to the angular position of the rotor. The advantages of micro VCM are that the stator electrodes can be either excited with DC or AC voltages. Frictional torque that is produced due to fabrication limitations imposed on the device construction is a serious drawback for the variable capacitance machines. However methods have been developed to combat this frictional torque. Figure 2.2 shows a micro variable capacitance machine (VCM).

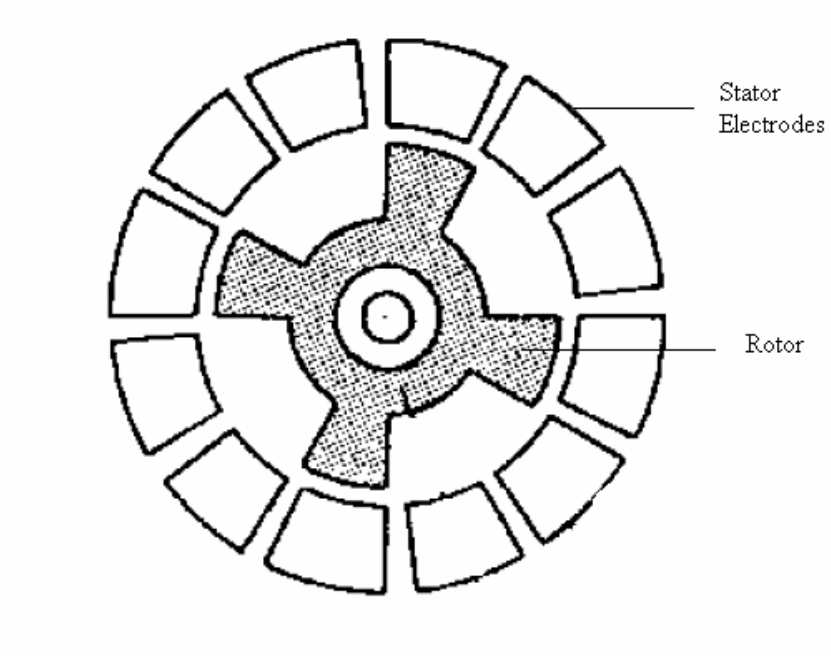

Figure 2.2 Electrostatic micro variable capacitance machine [8]

2) Electrostatic Induction Micro-motors: An electrostatic induction micro-motor is an asynchronous machine. Its principle of operation is based upon the charge relaxation to establish its rotor charge distribution as compared to the physical saliency

in case of variable capacitance micro-motors. Thus, rotor is a uniform conductor. A poly phase voltage source is used to apply potential to the stator electrodes. As the voltage is applied, the potential wave travels around the stator which in turn induces free electric image charges on the rotor surface. These image charges travel in synchronism with the potential wave, but due to charge relaxation in the rotor and stator-rotor air gaps, they lag behind. The resultant displacement between the stator potential wave and the image charges give rise to a motive torque acting on the rotor. The amount of motive torque depends upon the charge relaxation time, which further depends upon the conductivity of the rotor. If the rotor has high conductivity, charge relaxation time would be smaller, thus the image charges are only slightly displaced from the stator potential waves and the motive torque is reduced. On the other hand, if the conductivity of rotor is very small, charge relaxation time would be too long, hence very little image charges are induced thereby reducing the motive torque. Also, motive torque vanishes at the synchronous velocity of the rotor. For lesser velocities, the image charges lag behind the stator potential waves and the resulting motive torque is positive. On the other hand, for greater velocities, the image charges are carried ahead of the potential waves by the rotor motion, hence the resultant motive torque is negative. The design of an induction micro-motor is more complex than a VCM design because VCM performance can be optimized by using the best available insulators and conductors, whereas for induction micro-motors an optimal set of IM material properties exist for a given IM geometry and excitation. Figure 2.3 shows an electrostatic micro induction machine (Axial Design).

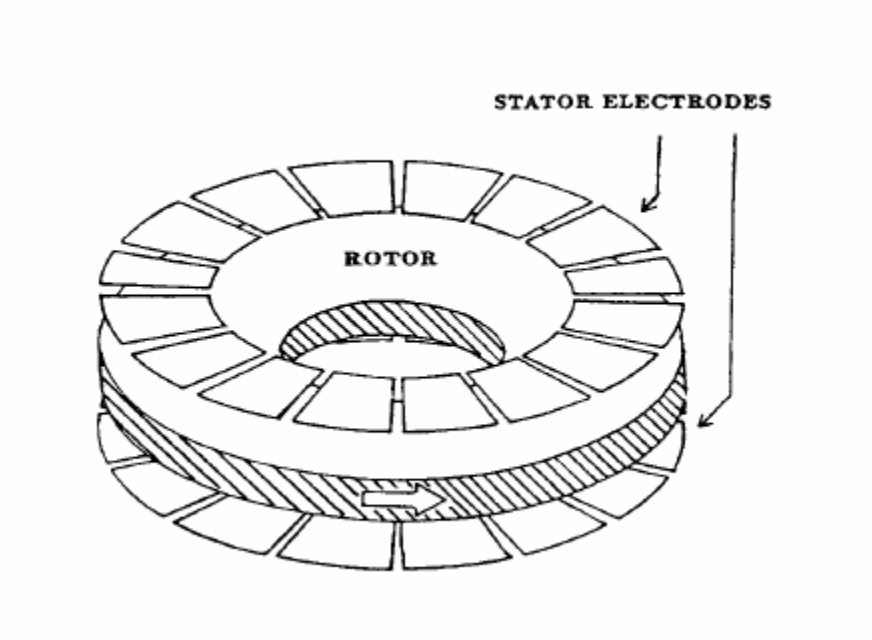

Figure 2.3 Electrostatic induction micro-machine [10]

3) Wobble Micro-motors: It is type of micro-motor that is based upon the wobbling action of the rotor. Its rotor is a smooth ring and uses the electrostatic attraction. The rotor rolls at the inner periphery of the stator electrode segments. The wobbling action follows a pattern in accordance to the excitation sequence of the stator segments. Also, axis about which the rotor rotates is not fixed but moves parallel to the stator axis and around it as it gets clamped to the stator segments. The advantages of wobble motor are reduced friction and higher torque at low speed. The disadvantage is that it is difficult to connect it to load. Figure 2.4 shows a wobble micro-motor.

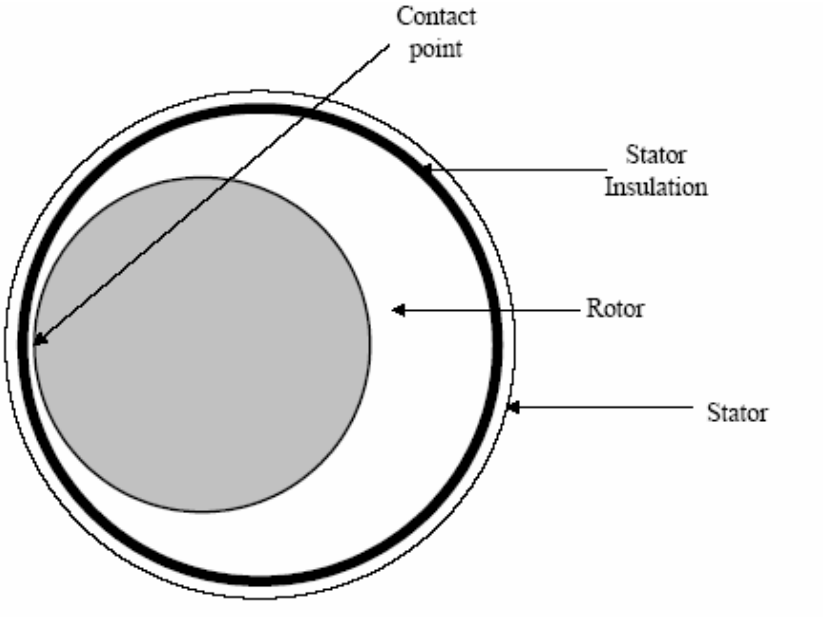

Figure 2.4 Wobble micro-motor [9]

Every electrostatic micro-motor has its own advantages and disadvantages. But for a preliminary investigation variable capacitance motor is considered to be most suitable because of its design and material requirement simplicity. Thus, this thesis has focused on the development of a variable capacitance micro-motor model. The following chapters cover the fundamentals of micro VCM, its analytical and dynamic modeling and finite element analysis in detail.

CHAPTER 3

FUNDAMENTALS OF MICRO VCM

A micro variable capacitance motor is an electromechanical energy converter. Its principle of operation is based upon a parallel plate capacitance model. Electrical energy is stored in the variable stator-rotor capacitance of the motor. The change in this energy in the direction of motion is proportional to the output torque of the motor.

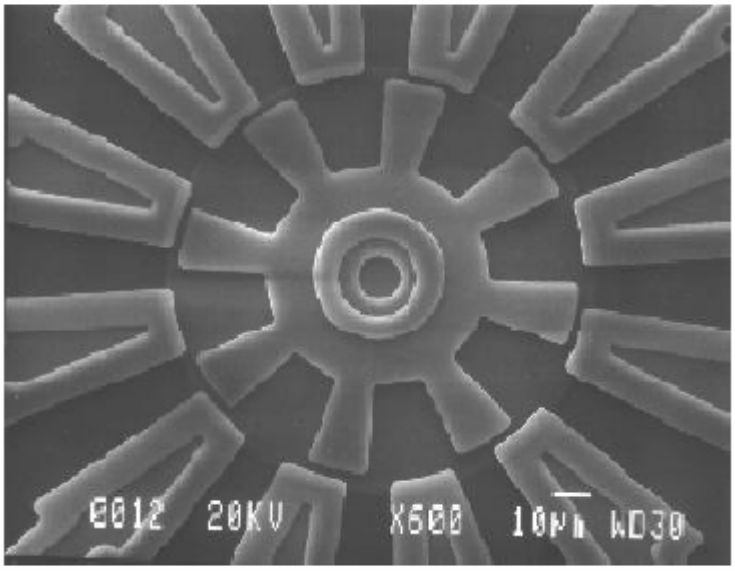

Figure 3.1 Micro variable capacitance motor (VCM) [11]

By definition, as the excitation is applied to the stationary pair of conducting stator electrodes, image charges are induced on the moving rotor (conductive) electrode. When these two conducting plates are slightly displaced with respect to each other, an electrostatic force is produced that has a component parallel to the surface of the

conducting plates that tends to realign the plates. This force is the motive force for the VCM. Once the rotor rotates and gets aligned with the excited stator electrodes, excitation to those stator electrodes is switched off so that the rotor continues to rotate. In the process of rotation as the next set of rotor poles reaches the stator electrodes, the excitation to the stator electrodes is switched on again. In this way the rotor and stator are synchronized in this type of actuation.

3.1 Equations Governing the Operation of the Micro VCM

Electrostatic energy stored in the stator-rotor capacitance is given by the following equation [12]:

$$W_e = \frac{1}{2} C V^2 \tag{3.1}$$

Where,

$W_e = Electrostatic\ energy\ stored\ in\ the\ stator-rotor\ capaci\tan ce$
$C = Stator-rotor\ capaci\tan ce$
$V = Applied\ stator\ voltage$

The torque of the micro VCM is proportional to the rate of change of electric energy stored with angular position, which is further proportional to the rate of change of stator-rotor capacitance with angular position i.e.

$$T = \frac{dW_e}{d\theta} \tag{3.2}$$

$$T = \frac{1}{2} V^2 \frac{dC}{d\theta} \tag{3.3}$$

$$C = \varepsilon_0 \varepsilon_r A / d \tag{3.4}$$

$\varepsilon_0, \varepsilon_r$, are the permittivity of air and relative permittivity of the dielectric respectively. A , is the area of overlap between stator and rotor poles, d is the separation between the stator and rotor electrode plates. Since area of overlap between the stator and rotor electrodes varies with position, stator-rotor capacitance also varies with position generating the motive torque thereby. Electric field in a variable capacitance machine does not saturate, but it is limited by the maximum breakdown strength of the air. Since, the dielectric is air there are no field losses in the air gap. The small mutual capacitances therefore do not contribute much to the field losses, thereby making capacitance versus position profile much more piecewise linear. Hence constant voltage results in constant torque.

3.2 Electrical Equivalent Circuit Model of a Micro VCM

A micro variable capacitance machine can be modeled as a capacitance in parallel with the resistance. Also, there exists an induced current load in the micro variable capacitance machine that contributes to the torque, which is analogous to the back emf in case of switched reluctance machine. Current drawn by one phase of the stator can be expressed as:

$$i = \frac{v}{r} + \frac{dq}{dt} \tag{3.5}$$

Since, parallel plate capacitance model is considered for a micro VCM, induced charge can be written as:

$$q = C(\theta_r)v \tag{3.6}$$

From equations (3.5) and (3.6)

$$i = \frac{v}{r} + \frac{d\left(C\left(\theta_r\right)v\right)}{dt} \tag{3.7}$$

$$i = \frac{v}{r} + C\left(\theta_r\right)\frac{dv}{dt} + v\,\frac{dC\left(\theta_r\right)}{dt} \tag{3.8}$$

$v, i, C\left(\theta_r\right), \theta_r, \omega_r$, represent stator phase voltage, phase current, stator-rotor capacitance at particular rotor position, rotor angular position and rotor angular velocity respectively.

$v\,\frac{dC\left(\theta_r\right)}{dt}$, is the induced current load, which can also be written as $v\,\omega_r\,\frac{dC\left(\theta_r\right)}{d\theta}$ and can be modeled as a voltage dependent current load.

Multiplying both sides of equation (3.8) with stator phase voltage v, we get

$$vi = \frac{v^2}{r} + vC\left(\theta_r\right)\frac{dv}{dt} + v^2\,\frac{dC\left(\theta_r\right)}{dt} \tag{3.9}$$

$$vi = \frac{v^2}{r} + vC\left(\theta_r\right)\frac{dv}{dt} + v^2\,\omega_r\,\frac{dC\left(\theta_r\right)}{d\theta} \tag{3.10}$$

From equation (3.3)

$$vi = \frac{v^2}{r} + vC\left(\theta_r\right)\frac{dv}{dt} + \omega_r T \tag{3.11}$$

Thus, it is clear from equation (3.11) that induced current load generates torque in micro variable capacitance machine, which when multiplied by angular speed of the rotor gives mechanical power. Figure 3.2 represents electrical equivalent circuit of the micro variable capacitance machine.

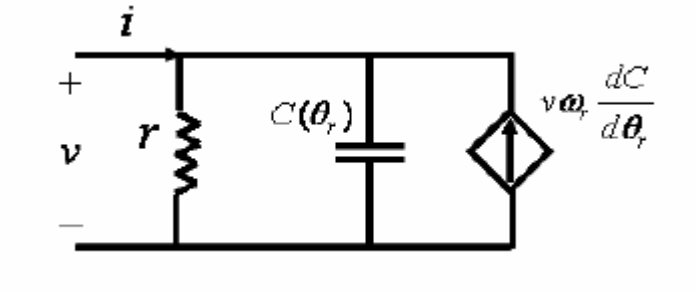

Figure 3.2 Electrical equivalent circuit of a micro VCM [12]

CHAPTER 4

FINITE ELEMENT ANALYSIS OF MICRO VCM

4.1 Design Procedure of Micro VCM

The design procedure of micro VCM is somewhat similar to its magnetic counterpart, switched reluctance machine. In this section design procedure of micro VCM has been discussed, which includes the selection of rotor and stator diameter, pole selection, rotor and stator pole angle selection.

By definition, a micro-motor should have the dimensions less than 1 mm in every direction. Thus, the inner and outer radii of stator and rotor have been selected by keeping this definition in mind. The inner and outer radii of stator are 0.3mm and 0.45mm respectively. Similarly, inner and outer radii for rotor are 0.147 and 0.297 mm respectively. The length of the air gap is 0.003mm. The pole selection for micro VCM is similar to that of switched reluctance machine. This thesis focuses on 8/6 micro VCM i.e. 8 stator poles and six rotor poles which a very popular combination for switched reluctance machines. The advantage of this combination is less torque ripple. The stator and rotor pole angle selection form a crucial part of the design procedure. Again it is similar to the switched reluctance machine. Various constraints on the stator and rotor pole angles can be summarized as follows:

1) Rotor pole angle β_r should be greater than stator pole angle β_s.

2) Stator pole angle β_s should be greater than the stroke angle which is defined as:

$$\varepsilon = \frac{2\pi}{\frac{N_s}{2} N_r}$$

Where N_s , N_r are number of stator and rotor poles.

If this is not the case, then there may be some positions in the machine from where the machine may not start.

3) The angle between the corners of adjacent rotor poles must be greater than the stator pole arc. Otherwise there will be an overlap between the stator and rotor poles in the unaligned position, due to which the machine starts having positive capacitance profile before reaching the minimum value. So, minimum value of capacitance increases which reduces the torque generated by the machine. This constraint can be expressed as:

$$\frac{2\pi}{N_r} - \beta_r > \beta_s$$

All these constraints, when represented graphically produce a feasible triangle. It is required that stator and rotor pole angles lie in this feasible triangle. Figure 4.1 shows the feasible triangle for an 8/6 micro VCM.

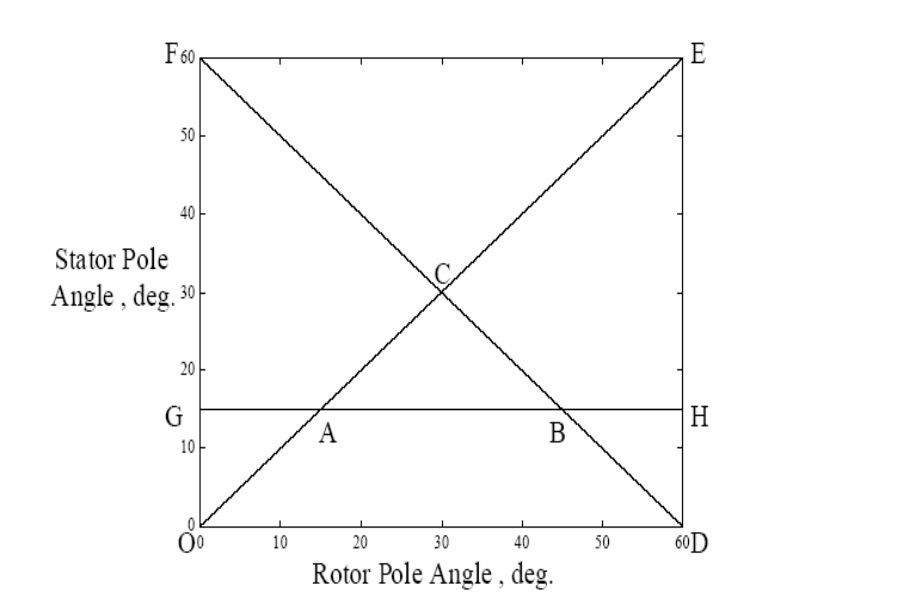

Figure 4.1 Feasible triangle for a 8/6 micro variable capacitance machine [13]

This triangle gives the restrictions on stator and rotor pole angles. However, a method to find optimum stator and rotor pole angles is still unexplored. In this thesis, finite element method has been used for this purpose. Finite element model of the micro VCM is developed first. Then torque profile for the machine is obtained, for all possible combinations of stator and rotor pole angles lying in the feasible triangle, using finite element analysis. In the end, optimum value of stator and rotor pole angles, which produce maximum torque, is obtained.

4.2 Basics of Finite Element Analysis

Micro-structures such as micro-motors are upcoming technical products in various areas. Thus, the accurate prediction of the physical behavior of theses devices is required to have the complete understanding of their working principles. Finite element is such an accurate and professional design method which enables the simulation of

complex microstructures to accurately predict their behavior. FEA can be used to study various problems such as electric, magnetic, mechanical and thermal fields. In this thesis, FEA has been used to study the micro-motors operated by electrostatic field.

4.2.1 FEA General Procedure

Finite element analysis can be distinguished in three steps, a pre process, a solution process and a post process.

4.2.1.1 Pre Process

A pre process has various steps as follows:

1) Model Drawing

2) Material Assignment

3) Assigning Boundary Conditions and Sources

4) Specify Executive Parameters

5) Solution Setup

1) Model Drawing: In this step basic geometry is created. Also, it is used to identify grouped objects.

2) Material Assignment: In this step materials are assigned to each object in the geometry from a library of materials provided. If some material is not there in the library, it is added to t he library by defining all the material properties.

3) Assigning Boundary Conditions and Sources: In this step, voltage or current sources are assigned to the objects in the geometry. Also, boundary conditions are specified, such as the behavior of the electric field at the edge of the problem region, and potentials on the surfaces of the objects or ground planes in t his step.

4) Specify Executive Parameters: Specify the solution parameters that need to be computed during the solution such as capacitance, force, torque, flux lines.

5) Solution Setup: In this step, criterion to compute the solution is specified or modified depending upon how fast the convergence of the solution is required. Also, there is an option to select adaptive analysis. If the adaptive solution is selected, simulator solves the problem iteratively, refining the regions of the mesh in which the larger error exists.

4.2.1.2 Solution Process

After assigning sources, boundary conditions, and materials, a solution is obtained in this process depending upon what solution setup has been chosen. Solution involves calculating static electric field, magnetic fields, core loss, forces, torques, and capacitances, inductances due to voltage distribution, permanently polarized material, charges, DC currents, static external magnetic fields and permanent magnets. Solution is calculated by solving the differential equations, representing the elements in the model.

4.2.1.3 Post Process

In this step, the solution obtained in the solution process is further analyzed to get required results, solution information is viewed. Flux density plots, plots of normal and tangential components of forces in the air gap, current density plots can be easily obtained from any commercial FEA package available in the market.

4.3 Model Development

A commercially available finite element solver “Maxwell 2D” has been used for the analysis and modeling purposes in this thesis. Maxwell 2D is an interactive software package for analyzing electric as well as magnetic fields in structures with uniform cross-sections and full rotational symmetry where the field patterns in the entire device can be analyzed by modeling the field patterns in its cross-section.

Electrostatic solver of Maxwell 2D enables the modeling and simulation of electrostatic micro machines. Thus, Maxwell 2D electrostatic solver has been used to develop the 2D finite element model of a four phase 8/6 micro variable capacitance machine to analyze the electric fields in the structure and get capacitance and torque data.

4.3.1 Model Drawing

First step is the model drawing using the in-built model drawing tool of Maxwell 2D. The geometry of the model consists of a 4 phase, 8/6 micro VCM structure having 8 stator electrodes and six rotor poles. The stator electrodes are arranged to have two electrodes per phase. The outer radii of the rotor and stator are 0.297mm and 0.45mm respectively. Stator and rotor arc lengths are 21 degrees and 23 degrees respectively. The length of the air gap between the stator and rotor is 0.003mm. The details of the machine dimensions are provided in the Appendix A. Figure 4.1 shows the finite element model of micro VCM.

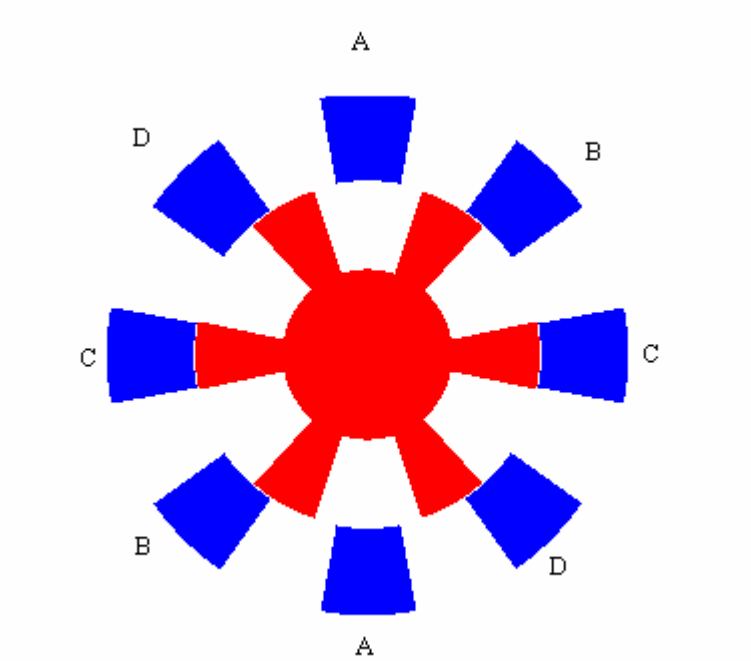

Figure 4.2 Finite element model of micro VCM

4.3.2 Material Assignment

The next step is the assignment of materials to all the objects in the finite element model. Material Assigned to rotor and stator electrodes is the same i.e. Poly Silicon. Since, this material is not present in the standard material library of the software; it is added as a user defined material in the library by defining its material properties and then assigned. Material assigned to the air gap is Air and material assigned to the background is Vacuum. Table 4.1 shows the material properties of Poly Silicon.

Table 4.1 Material Properties of Poly Silicon

Name	Poly Silicon
Relative Permittivity	11.7
Conductivity	0.00043478

4.3.3 Assignment of Sources and Boundary Conditions

The next step is to assign the sources to the objects in the geometry. Voltage excitation is provided to the stationary stator electrodes and rotor is grounded. Voltage of 300 volts is used as excitation voltage. Any of the four phases can be excited depending upon the requirement to get the desired torque and capacitance data.

4.3.4 Setting Executive Parameters

The next step is to set the parameters that need to be calculated e.g. capacitance matrix and torque on the rotor in this case when the excitation is applied to the stationary stator electrodes and rotor is rotated at a speed of 50,000 rpm.

4.3.5 Solution Setup

In this step, set the solution parameters. E.g. adaptive analysis will be selected so that the problem is solved iteratively, refining the regions of the mesh in each step.

After setting all the parameters and assigning the materials and boundary conditions to the developed model, 2D electrostatic solver would be used to get capacitance and torque profiles for a particular phase of VCM.

4.4 Optimum Stator and Rotor Pole Angle Selection

As explained above, to get optimum stator and rotor pole angles, torque profile of the micro VCM is obtained for different combinations of stator and rotor pole angles. Initially the machine is in the unaligned position with respect to phase A. Voltage excitation of 300V is applied to both the electrodes of phase A and the rotor is grounded. Setting for calculating rotor torque is done in the executive parameters settings. Mechanical speed of micro VCM is 50,000 rpm.

4.4.1 Simulation Results

Figure 4.3 shows torque profile for different combinations of stator and rotor pole angles viz. (30, 30), (18, 24), (20, 22), (20, 24), (20, 20), (20, 30), (21, 23) and (25, 25).

An investigation of figure 4.3 reveals that (30, 30) produces maximum torque. But, this pole combination does not satisfy third and first restrictions explained above. Pole combination (25, 25) also produces high torque. But, with this combination there can be a position where rotor pole will be overlapping with two stator poles so a negative torque will be produced if the voltage removal from the excited phase is not fast enough. Amongst all other combinations (21, 23) produces maximum torque and also satisfies all the restrictions. With this combination, at any position rotor pole will not overlap with two coinciding stator poles at the same time. Thus, it is considered the optimum combination of stator and rotor pole angles in this thesis.

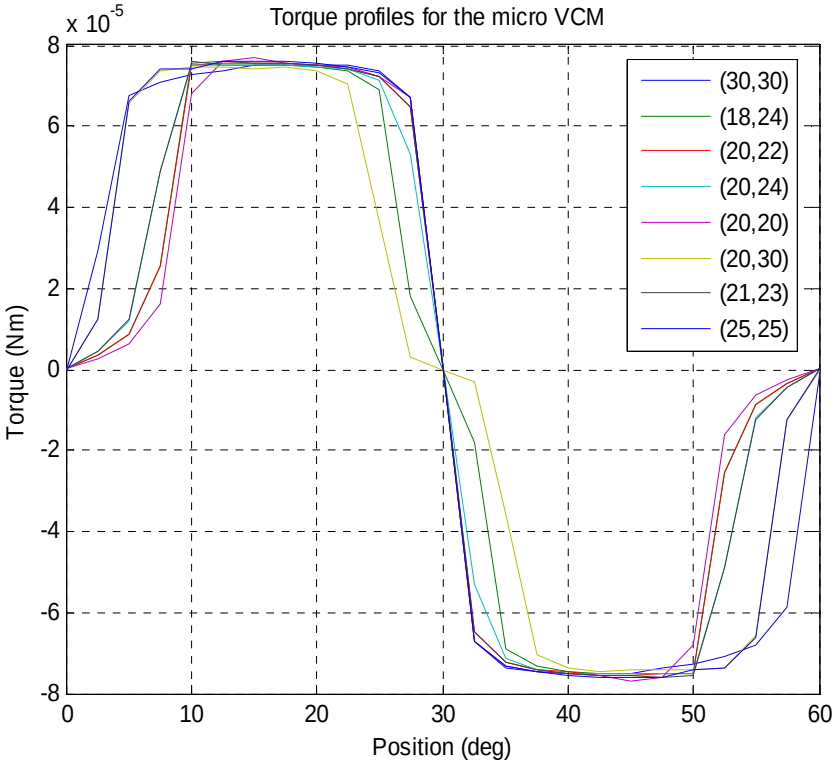

Figure 4.3 Torque profile for various stator and rotor pole angle combinations

4.5 Capacitance and Torque Calculation for FE Model

This section studies the capacitance and torque profile for each phase of the finite element model of the micro VCM. Initially the machine is in the unaligned position with respect to phase A. Voltage excitation of 300V is applied to both the electrodes of phase A and the rotor is grounded.

As the excitation is applied to phase A, rotor would move from unaligned to aligned to unaligned position over a period of one electrical cycle i.e. 60 degrees mechanical. The capacitance and torque profile of the VCM over one electrical cycle are shown in figures 4.4 and 4.5 respectively.

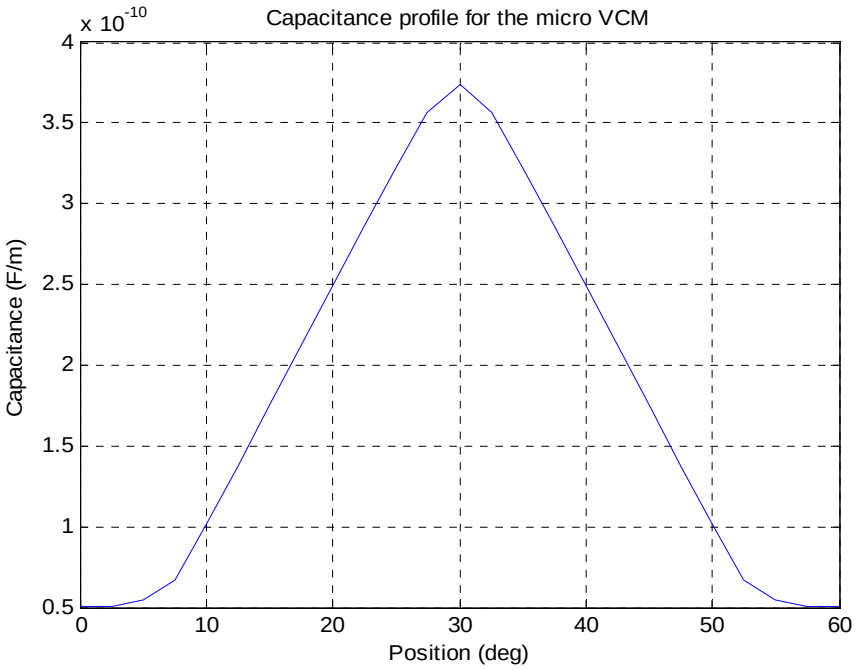

Figure 4.4 Capacitance profile of micro VCM

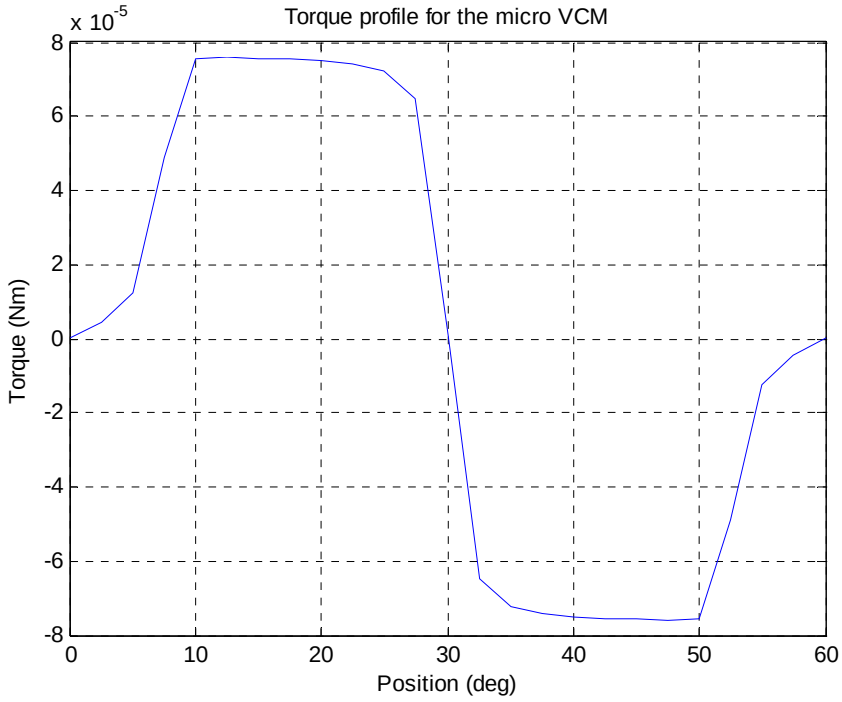

Figure 4.5 Torque profile of micro VCM

4.5.1 Unaligned Position

The micro VCM is said to be in unaligned position with respect to a particular phase, when the inter-polar axis of the rotor gets aligned with the stator poles of that phase. In this position, there is no overlapping between the rotor poles, and stator poles of that particular phase. Now as capacitance is directly proportional to the area of overlap of two charged plates, stator-rotor capacitance at this position will be the minimum which is evident from figure 4.4. Also, torque on the rotor will be the maximum at unaligned position as shown in figure 4.5 because rotor poles are displaced maximum from the stator poles of the excited phase.

4.5.2 Aligned Position

The micro VCM is said to be in aligned position with respect to a particular phase, when any pair of rotor poles is exactly aligned with the stator poles of that phase. In this position, there is complete overlap between the rotor poles, and stator poles of that particular phase. Thus, stator-rotor capacitance at aligned position will be the maximum as shown in figure 4.4. Also, the excited phase produces no torque until it is displaced to either of sides i.e. torque on the rotor will be zero as shown in figure 4.5

4.6 Effects of Machine Geometry on Capacitance and Torque Profiles

A number of independent parameters define the geometry of the machine such as rotor diameter, stator arc length, rotor arc length, air gap length, number of stator and rotor poles etc. The most important are rotor and stator arc length and air gap length. In this section, influence of variation in these parameters on capacitance and torque profiles of the machine has been discussed.

4.6.1 Width of Stator and Rotor Arcs

The influence of varying stator and rotor arc widths on capacitance and torque profiles of the VCM has been studied earlier.

4.6.2 Rotor Arc Length with Fixed Stator Arc Length

Figures 4.6, 4.7, show the effect of changing rotor arc length, while the stator arc length is fixed, on capacitance and torque profiles of micro VCM. As the rotor arc length increases from 23 to 27 degrees , with fixed stator arc length of 21 degrees, width of the aligned position increases resulting in larger overlapped area between stator and rotor. Thus, the torque characteristics shift away from the aligned position.

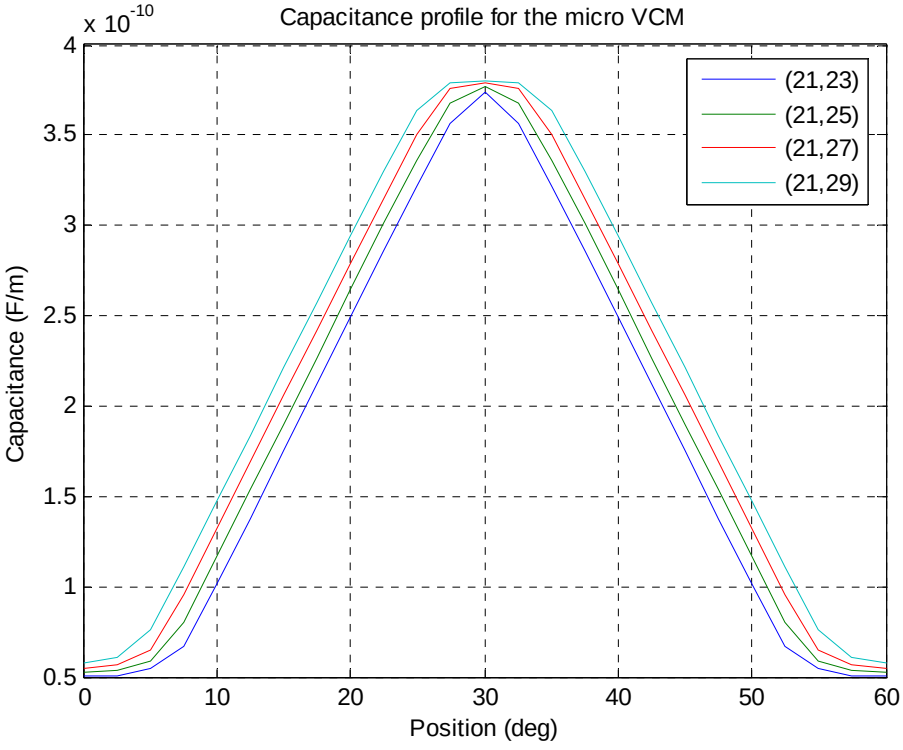

Figure 4.6 Capacitance profile of micro VCM for varying rotor arc length

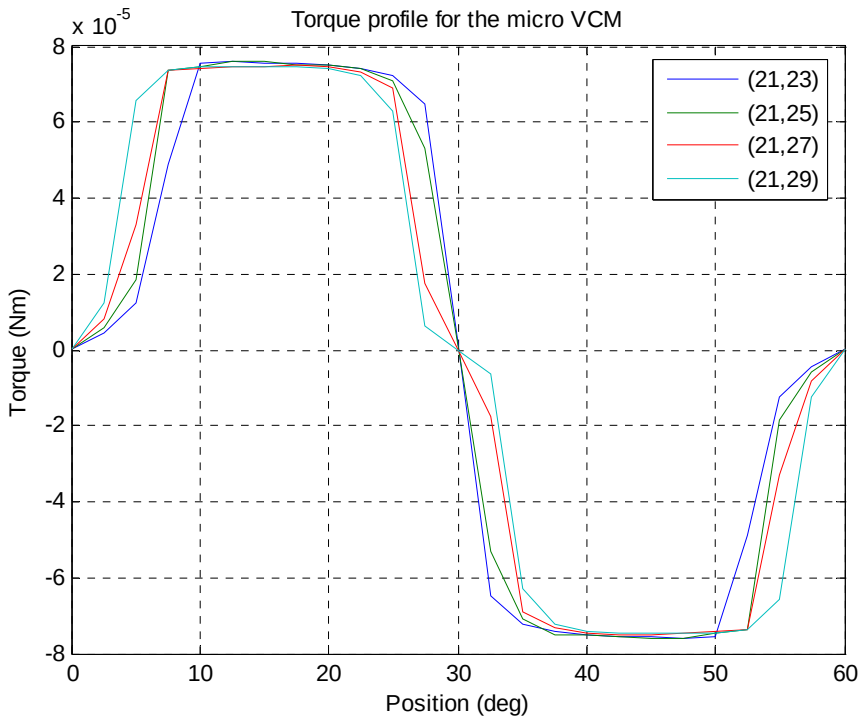

Figure 4.7 Torque Profile of Micro VCM for varying Rotor Arc Length

4.6.3 Length of Air Gap

Since the stator-rotor capacitance is inversely proportional to the distance between the stator and rotor electrode plates form equation (3.4), the phase capacitance increases as the air gap length decreases. Thus phase capacitance varies inversely with air gap length. Similarly, torque is also inversely proportional to the air gap length. Figures 4.8, 4.9, show the variation of phase capacitance, and torque as the air gap length varies from 0.003mm to 0.006mm.

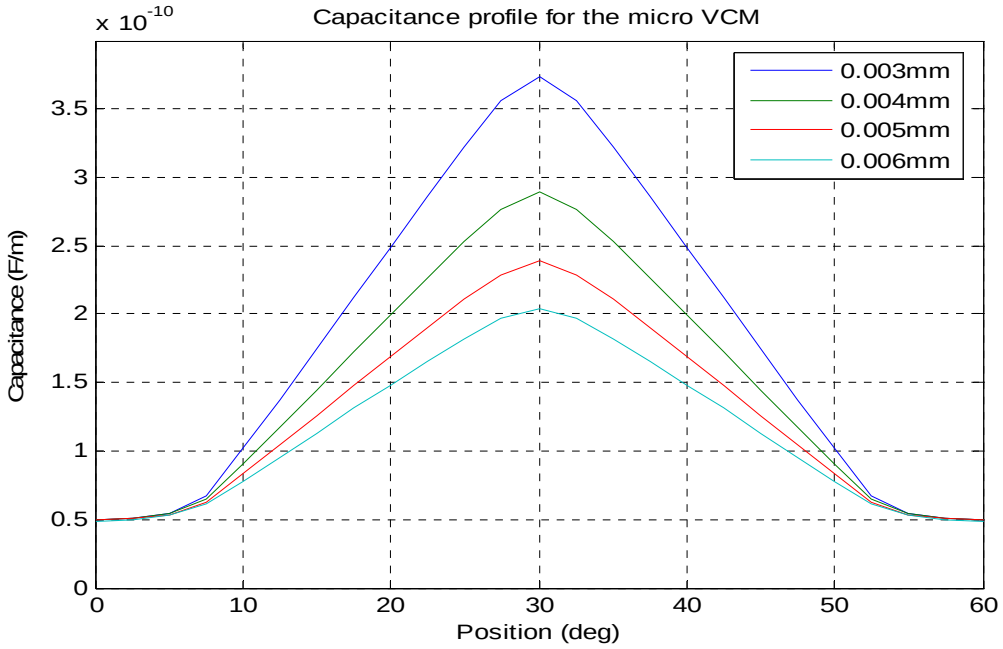

Figure 4.8 Capacitance profile of micro VCM for varying air gap length

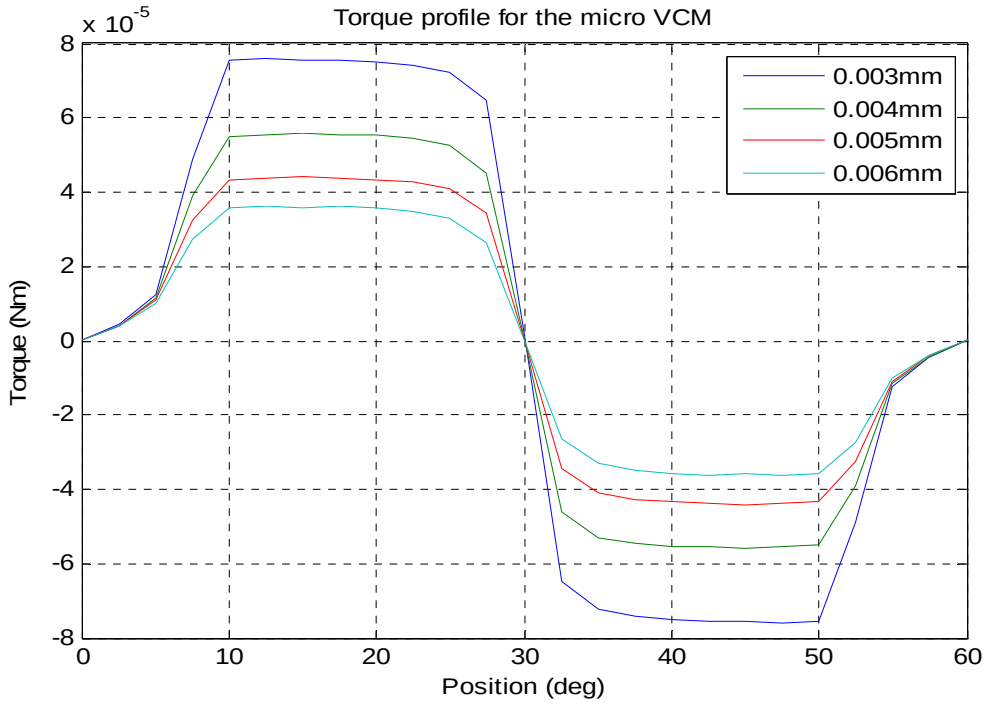

Figure 4.9 Torque profile of micro VCM for varying air gap length

The decrease in air gap length is limited by the electric breakdown limit of the air gap, which also puts an upper limit on the applied voltage excitation. Applied voltage excitation is fixed to 300 Volts.

4.7 Electric Flux Density Distribution

It is interesting to observe the behavior of tangential and normal flux density in the air gap of the machine, when the machine is under excitation. Figure 4.10 shows the tangential component of electric flux density (D_t) in the air gap of the machine, when phase A of the machine is excited with a voltage of 300 volts and it is at unaligned position with respect to phase A. Figure 4.11 shows the normal component of electric flux density (D_n) in the air gap of the machine under same conditions.

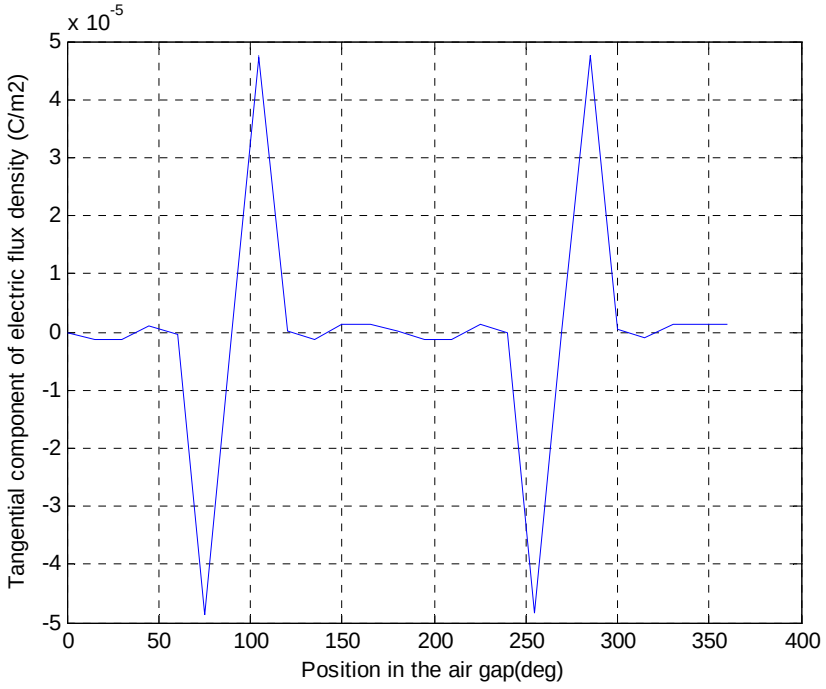

Figure 4.10 Tangential component of electric flux density in the air gap

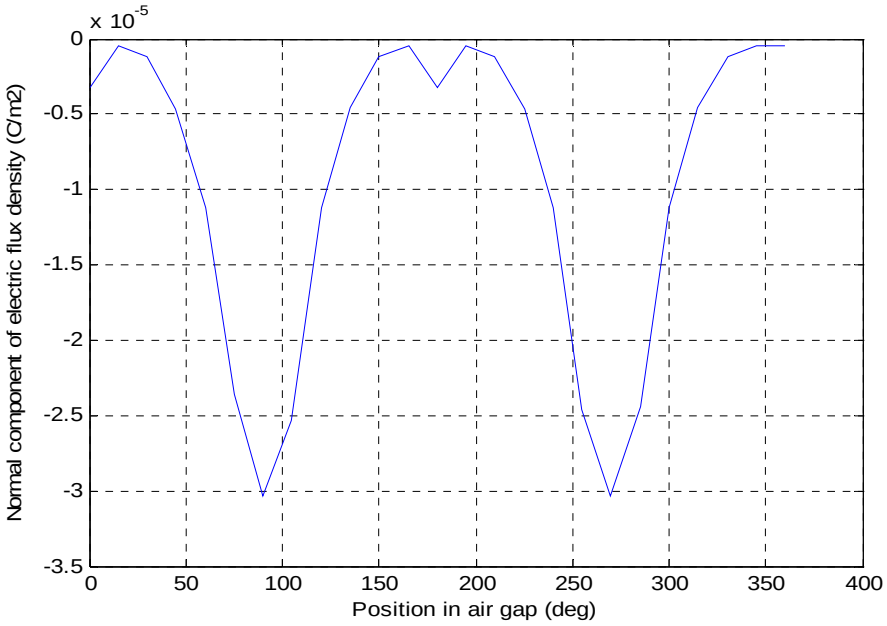

Figure 4.11 Normal component of electric flux density in the air gap

Figure 4.12 and 4.13 show the tangential and normal components of electric flux density in the air gap, when the phase A of the machine is excited with a voltage of 300 volts and it is at a position midway between the aligned and the unaligned position with respect to phase A.

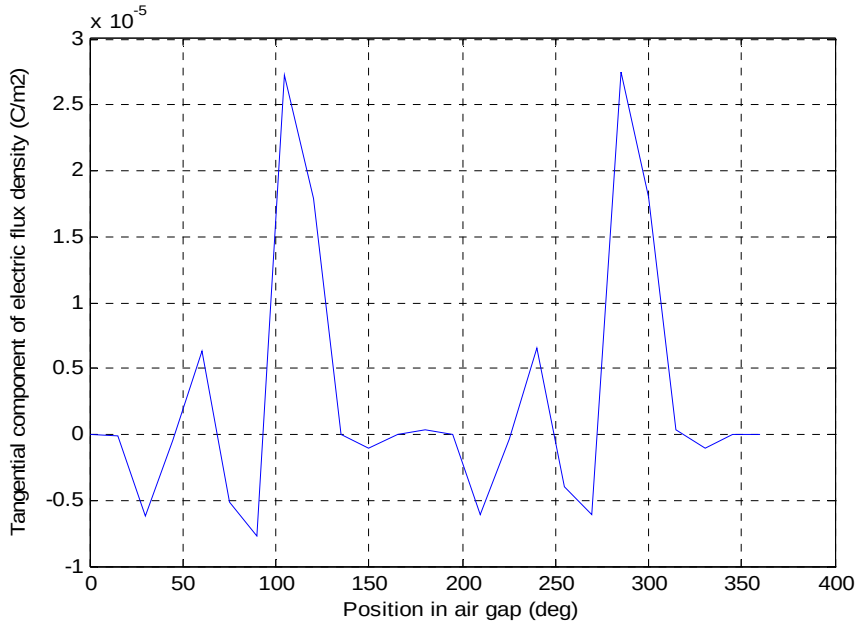

Figure 4.12 Tangential Component of Electric Flux Density in the air gap

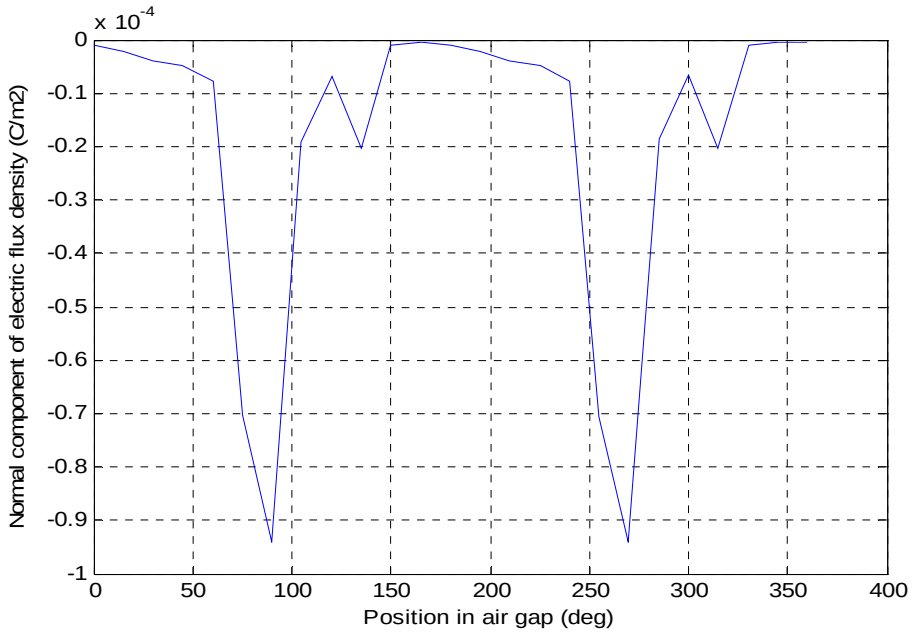

Figure 4.13 Normal component of electric flux density in the air gap

Figure 4.14 and 4.15 show the tangential and normal components of electric flux density in the air gap respectively, when the machine is excited with a voltage of 300 volts and it is at aligned position with respect to phase A.

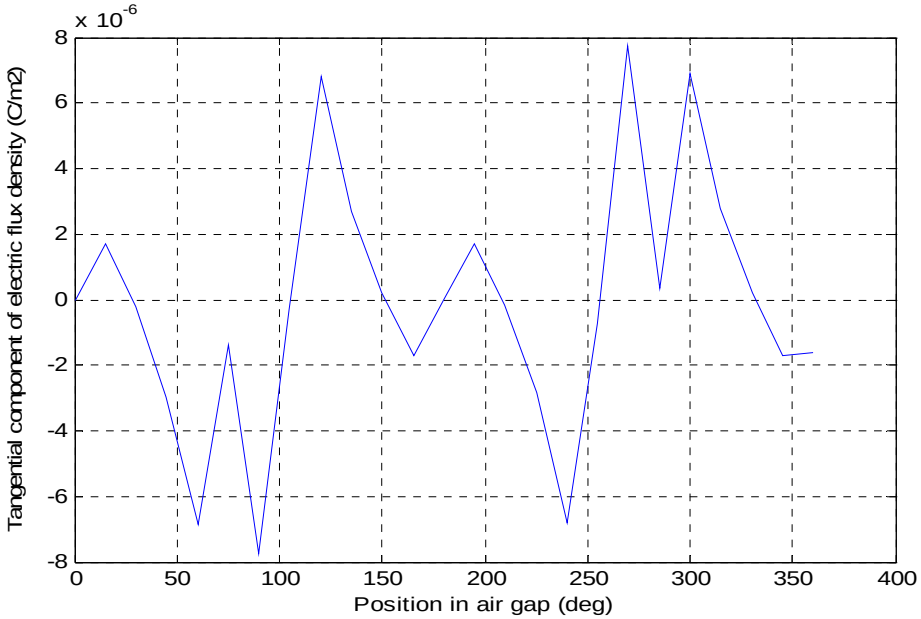

Figure 4.14 Tangential component of electric flux density in the Air Gap

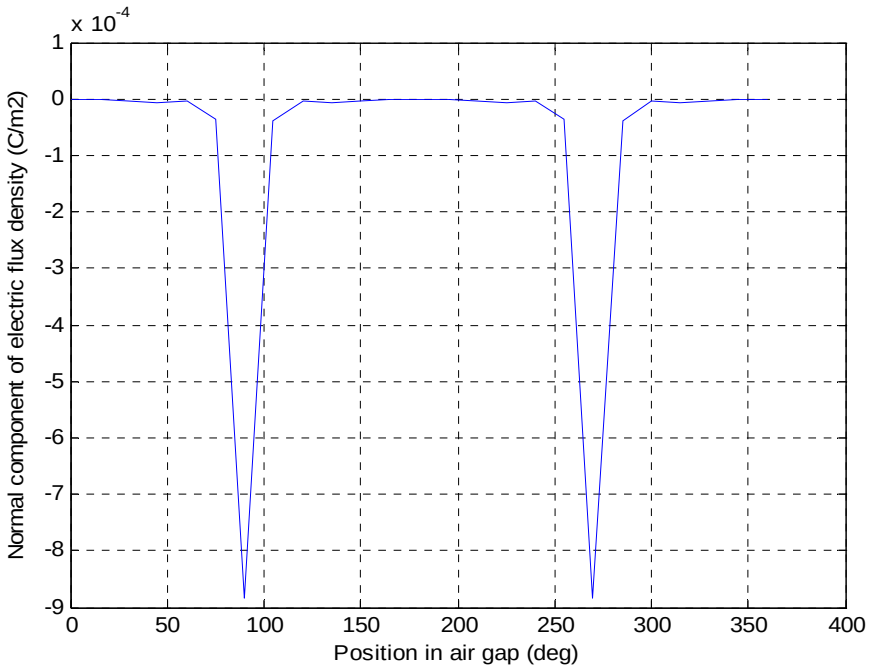

Figure 4.15 Normal component of electric flux density in the air gap

Figures 4.16, 4.17 and 4.18, show the D field distribution at the rotor –stator interface of the machine at various rotor positions respectively, when phase of the machine is excited with 300 volts.

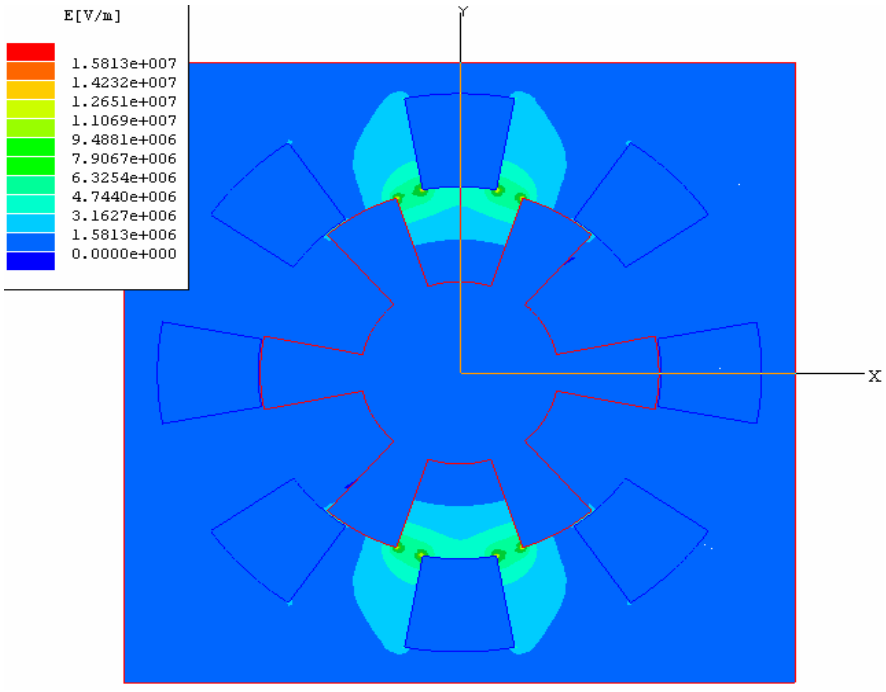

Figure 4.16 D-Field distribution in the machine at unaligned position

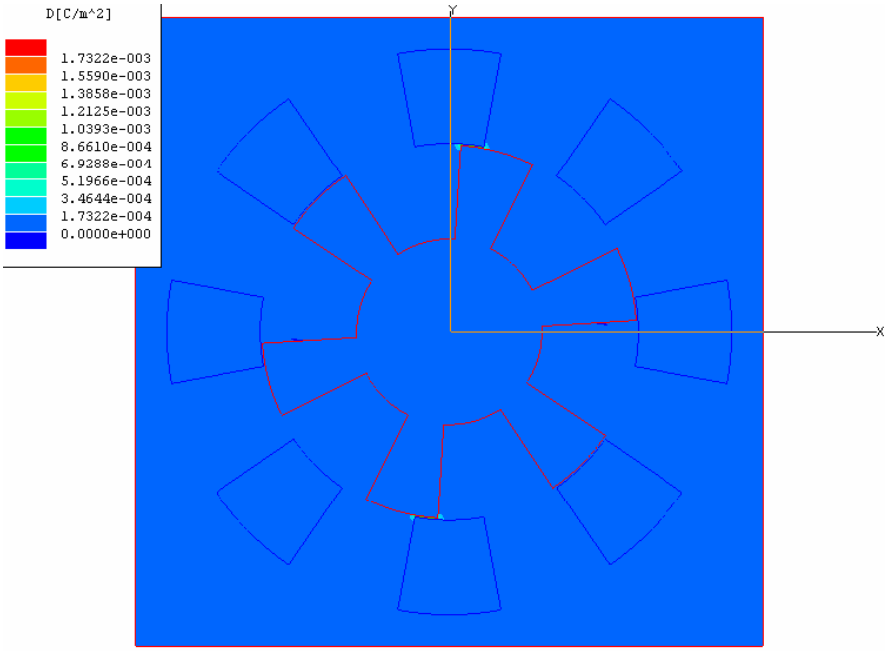

Figure 4.17 D-Field distribution in the machine at position midway between the aligned and unaligned Position

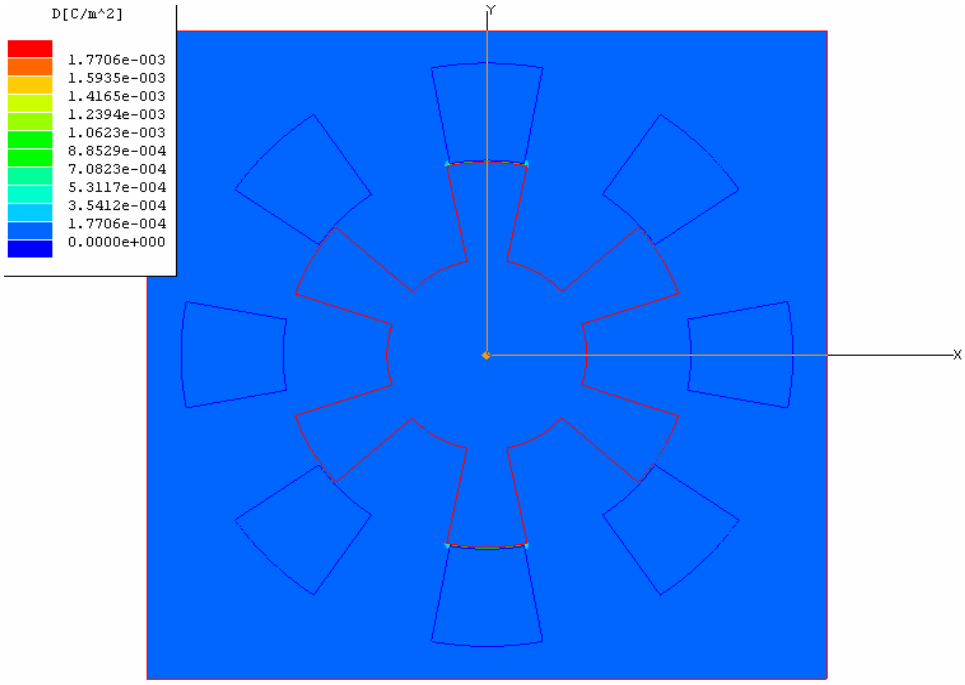

Figure 4.18 D-Field distribution in the machine at aligned position

4.8 Stress Tensor Method

Various methods can be used for the computation of electrostatic forces in an electromechanical energy conversion device. The most commonly used methods are:

1) Co-Energy Method

2) Stress Tensor Method

In the Co-Energy method, the tangential component of the electrostatic force is calculated by differentiating the total co-energy with respect to the position of the rotor. This method has been employed above to calculate the torque generated in the VCM for single phase excitation. This method provides a relatively straight forward solution to the problem. However, it does not give an insight into the distribution of the radial and tangential components of the electrostatic force in the air gap of the machine.

Maxwell stress tensor method provides such flexibility by providing a numerical technique for computation of the radial and tangential components of the electrostatic force densities at every point on a closed contour located in the air gap of the machine. This method is based upon the expression for electrostatic force density, f acting on charged bodies having constant permittivity i.e.

$$f = \rho E \tag{4.1}$$

Where ρ, is the volume charge density and E is the electric field strength [14].

The electric force density f is a vector quantity having components in different directions of the co-ordinate system. Thus, the resultant electrostatic force acting on a charged body in one direction can be found by integrating the electric force density over its volume in that particular direction. The ith component of the resultant electrostatic force can be expressed by the following expression:

$$F_i = \int_V \rho E_i \, dV \tag{4.2}$$

Now, Poisson's equation in electrostatics is:

$$\nabla . (\varepsilon_o E) = \rho$$

Where ε_o is the permittivity of free space. (4.3)

Substituting value of ρ form equation (4.3) into equation (4.2)

$$F_i = \int_V \nabla . (\varepsilon_o E) E_i \, dV \tag{4.4}$$

The Maxwell stress tensor is defined as:

$$\nabla . T_i = \nabla . (\varepsilon_o E) E_i \tag{4.5}$$

The vector T in equation (4.5) can be written as:

$$T_i = T_{i1}\, e_1 + T_{i2}\, e_2 + T_{i3}\, e_3 \tag{4.6}$$

Where e_i is a unit vector in some arbitrary orthogonal co-ordinate system. Substituting equation (4.5) into equation (4.4) and converting the volume integral into a surface integral enclosing the volume V by using Gauss's divergence theorem, the following expression will be obtained:

$$F_i = \int_V T_i \,.\, n\, dS \tag{4.7}$$

Where n is the unit normal vector pointing in the outward direction of the enclosing surface S. The components of the Maxwell stress tensor are given by:

$$T_{ij} = \varepsilon_o\, E_i\, E_j - \frac{\varepsilon_0}{2} E^2\, \delta_{ij} \tag{4.8}$$

Where δ_{ij} is the Kronecker delta and where the electric field is field in the surrounding media at the surface of the object. For a cylindrical system, with co-ordinates r, ϕ and z, the Maxwell stress tensor in equation (4.8) can be explicitly written as the following (3 × 3) matrix:

$$\frac{\varepsilon_o}{2} \begin{bmatrix} E_r{}^2 - E_\phi{}^2 - E_z{}^2 & 2E_r E_\phi & 2E_r E_z \\ 2E_r E_\phi & -E_r{}^2 + E_\phi{}^2 - E_z{}^2 & 2E_\phi E_z \\ 2E_r E_z & 2E_\phi E_z & -E_r{}^2 + E_\phi{}^2 + E_z{}^2 \end{bmatrix} \tag{4.9}$$

Since, in a two – dimensional problem there is no z component; matrix in equation (4.10) reduces to a (2 × 2) tensor matrix.

$$T_{ij} = \begin{bmatrix} T_r \\ \\ T_\phi \end{bmatrix} = \frac{\varepsilon_o}{2} \begin{bmatrix} E_r^{\,2} - E_\phi^{\,2} & 2E_r E_\phi \\ \\ 2E_r E_\phi & -E_r^{\,2} + E_\phi^{\,2} \end{bmatrix} \tag{4.10}$$

The radial and tangential components can then be written as follows:

$$T_r = \frac{1}{2}\,\varepsilon_o \left(E_r^{\,2} - E_\phi^{\,2}\right) \tag{4.11}$$

$$T_\phi = \varepsilon_o\, E_r\, E_\phi \tag{4.12}$$

T_r, is the radial stress which tries to reduce the air gap length by attracting the stator and rotor poles towards each other, T_ϕ is the tangential stress which tries to reduce the air gap separation by increasing the pole overlap area. By integrating these stresses over the closed contour (considering a 2 D problem) located in the air gap of the machine, total tangential and normal forces acting on the stator and rotor can be computed. When there is complete overlap of stator and rotor poles, and the air gap is uniform, integration of T_r and T_ϕ over the closed contour enclosing the rotor will be zero. Also, as T_r is directed along the center, no torque is produced by this component; all torque is produced by the tangential component of stress. The torque surface density developed by tangential stress is given by:

$$t = r \times T_\phi \tag{4.13}$$

4.9 Force Calculation in Finite Element Model

The Maxwell stress tensor method described above is used to calculate the normal and tangential force components over a closed contour located in the middle of the air gap at a particular rotor position. The process is repeated to obtain the forces for various rotor positions viz. Unaligned, Aligned, and midway between Aligned and Unaligned rotor positions.

4.9.1 Simulation Results

Figures 4.19 and 4.20 show the tangential and normal components of electric forces over a closed contour located in the middle of the air gap of the machine respectively for unaligned position, aligned position and position midway between aligned and unaligned.

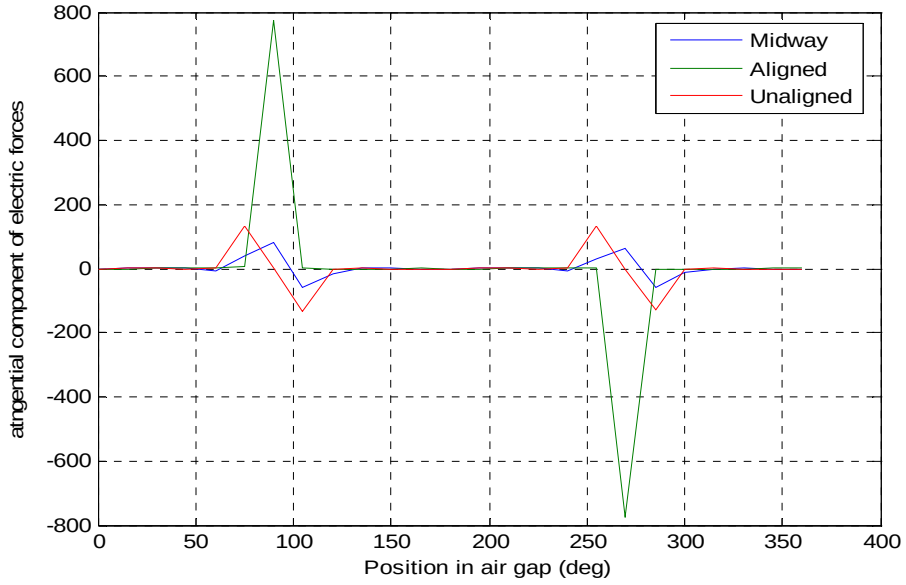

Figure 4.19 Tangential components of electric forces in the air gap of the machine for aligned, unaligned and midway positions

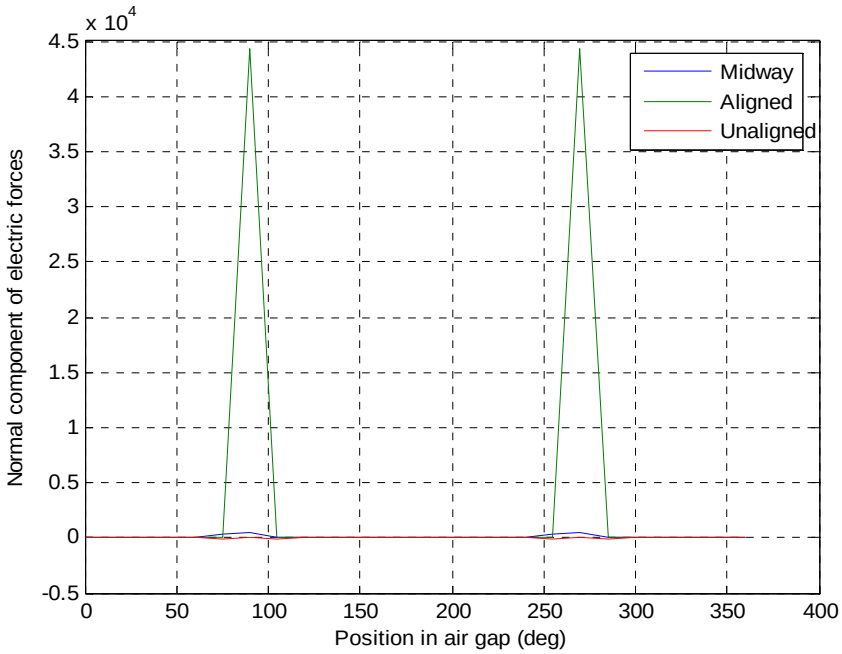

Figure 4.20 Normal components of electric forces in the air gap of the machine for aligned, unaligned and midway positions

4.10 Study of Mutual Effects

It is interesting to investigate the effects of mutual flux between two adjacent phases of the micro VCM, excited at the same time, on tangential and normal components of forces in the air gap of the machine. To study this effect, tangential and normal components of the electric forces in the air gap of the machine are calculated when:

1) Phase A of the machine is excited

2) Phase D of the machine is excited

3) Phase A and Phase D of the machine are excited simultaneously

The rotor of micro VCM is at an angle of 7.5 degrees to the unaligned position with respect to phase A of the machine. Figure 4.21 and 4.22 show the tangential and

normal components of force in the air gap of the machine respectively, for three different excitations as explained above, with rotor at 7.5 degrees.

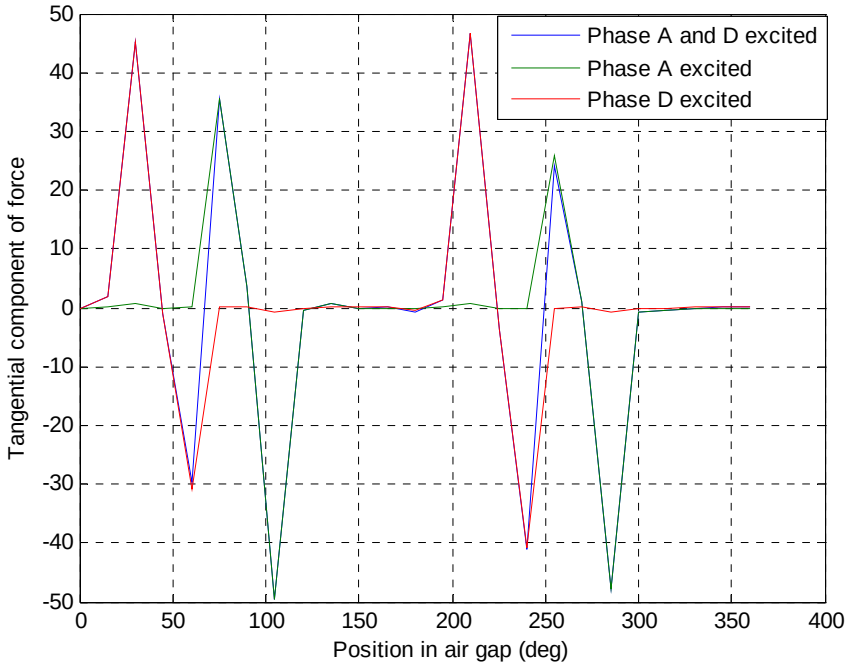

Figure 4.21 Tangential components of forces in the air gap for three different excitations with rotor at 7.5 degrees

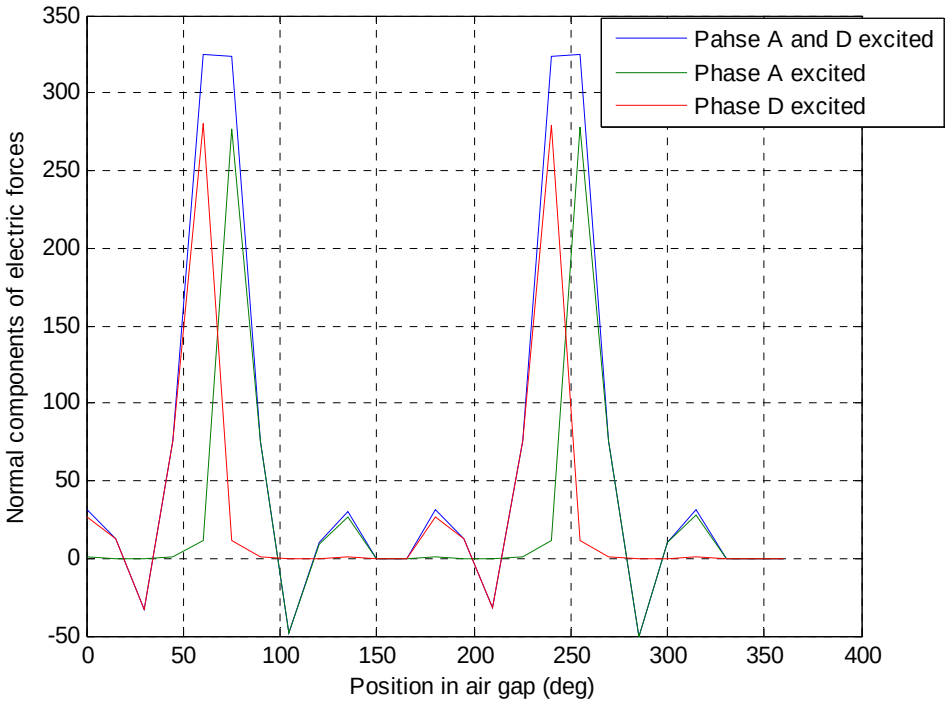

Figure 4.22 Normal components of forces in the air gap for three different excitations with rotor at 7.5 degrees

Now, the tangential components of forces with Phase A excited are added up with the tangential components of forces with Phase D excited, and compared with the tangential components of forces with Phase A and Phase D excited simultaneously. The rotor is at 7.5 degrees. Figure 4.23 illustrates this comparison. Same comparison is done for normal components of electric forces, as illustrated in figure 4.24

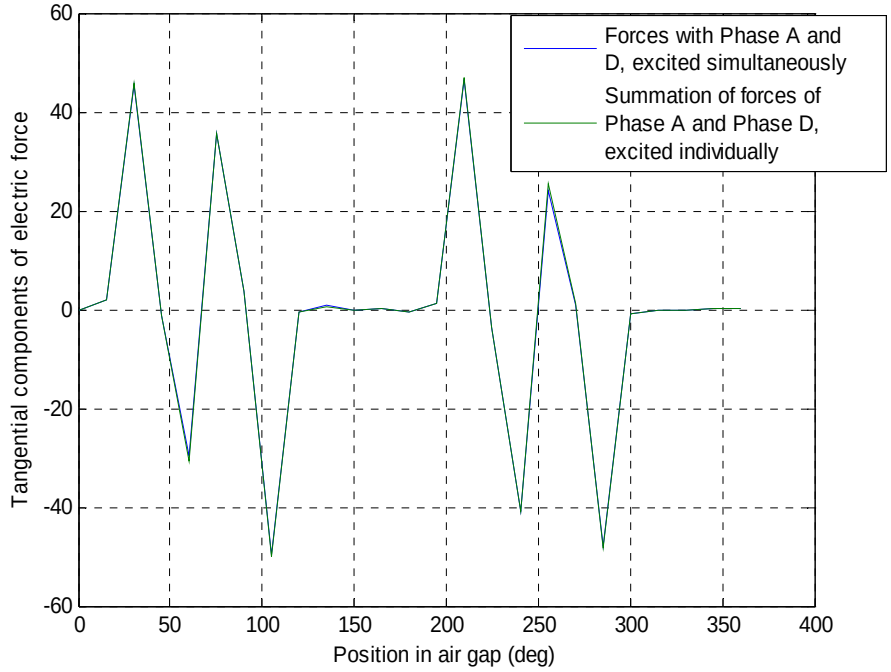

Figure 4.23 Comparison of tangential components of electric forces

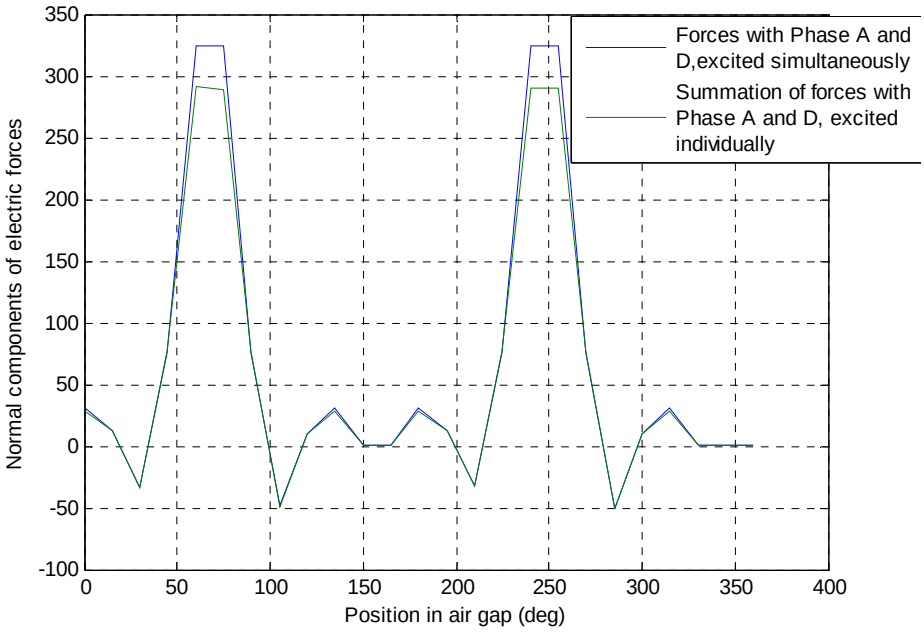

Figure 4.24 Comparison of normal components of electric forces

It is evident from the two figures that the summation curve for individual phase excitation does not differ much from the curve with simultaneous phase excitation. Thus the mutual effects of flux in the micro VCM are very small. So, it is valid assumption to consider no mutual effects in micro VCM, while calculating the phase capacitance and torque for the machine.

Same assumption is verified by considering the rotor at 22.5 degrees to unaligned position of the machine with respect to phase A. In this case also similar excitation sequence is followed for the same two adjacent phases, A and D, of the machine. Figure 4.25 and 4.26 show the tangential and normal components of force in the air gap of the machine respectively, for three different excitations as explained above, with rotor at 22.5 degrees.

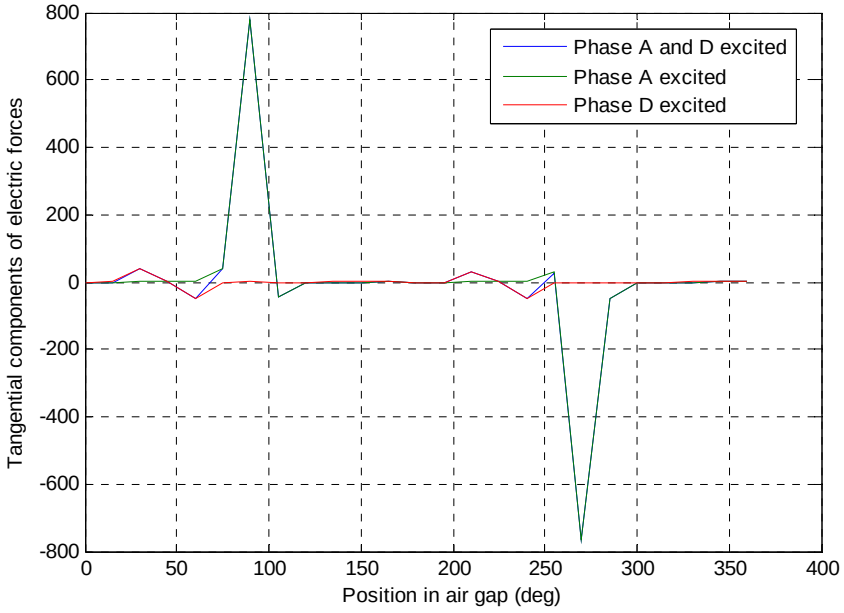

Figure 4.25 Tangential components of forces in the air gap for three different excitations with rotor at 22.5 degrees

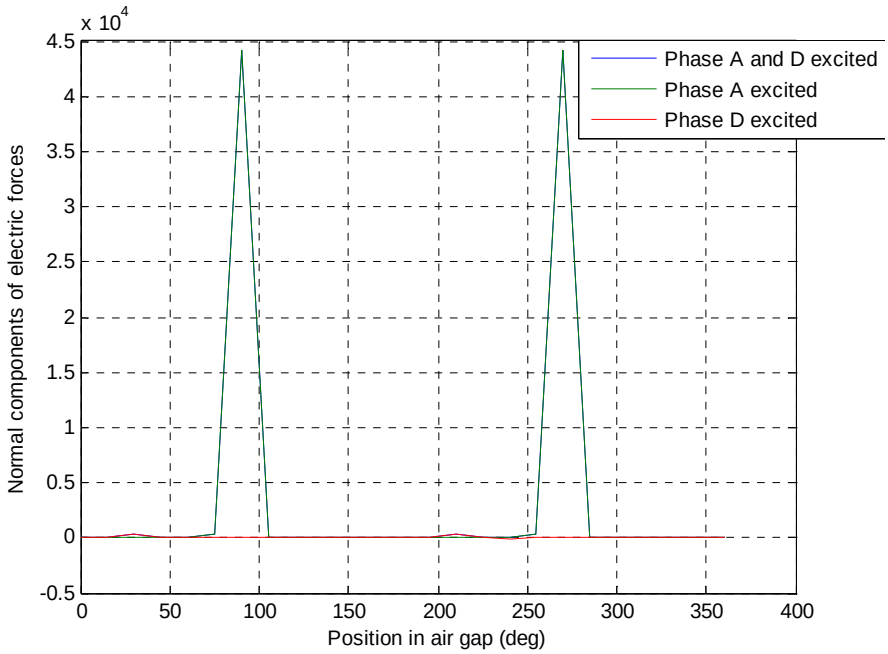

Figure 4.26 Normal components of forces in the air gap for three different excitations with rotor at 22.5 degrees

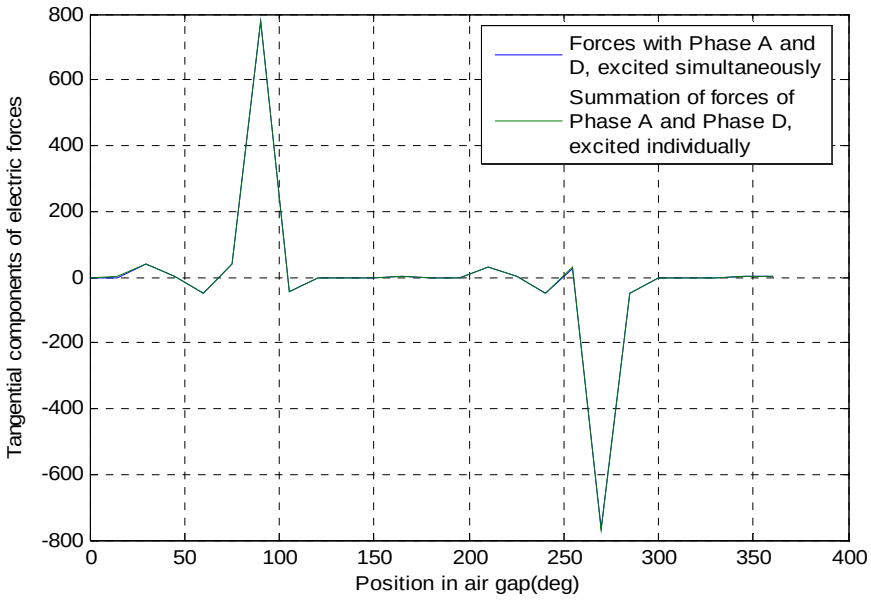

Figure 4.27 Comparison of tangential components of electric forces

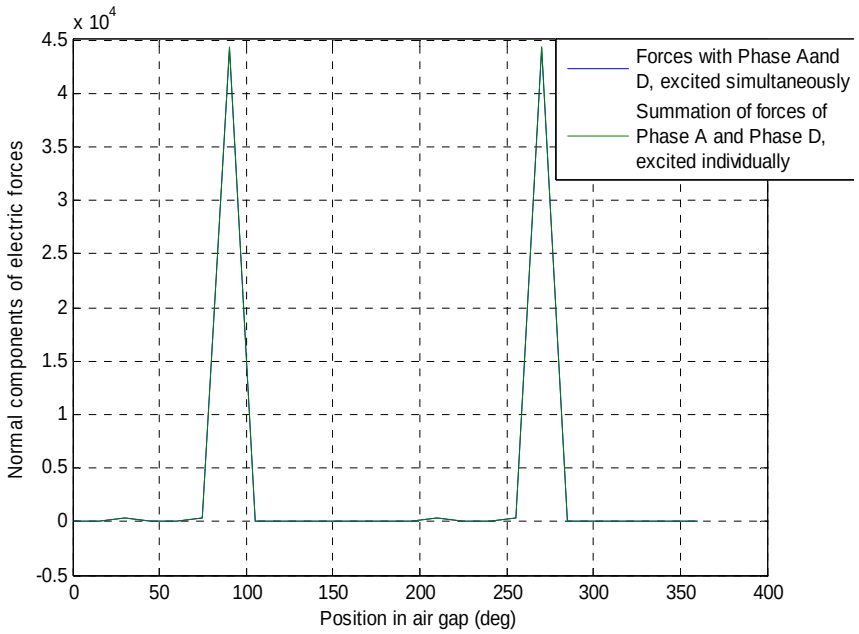

Figure 4.28 Comparison of normal components of electric forces

Thus, it is clear from the figures again, that mutual effects of electric fluxes are very small. So the assumption of considering no mutual effects is a valid assumption.

CHAPTER 5

MODELING OF PHASE CAPACITANCE AND TORQUE

5.1 Fourier Series Representation of Phase Capacitance

As clear from the finite element analysis of micro VCM, its phase capacitance is a periodic function of the rotor position. Thus, it is valid assumption to relate the phase capacitance of the micro VCM with rotor position by means of a Fourier series [15],

$$C(\theta) = \sum_{n=0}^{\infty} C_n \, Cos(n N_r \, \theta + \phi_n) \tag{5.1}$$

Where,

N_r = *Number of rotor poles*
θ = *Rotor Position*
$C(\theta)$ = *Phase Capacitance at any rotor position*

Considering the first five terms of the Fourier series in equation (5.1),

$$C(\theta) = C_0 + C_1 \, Cos(N_r \, \theta) + C_2 \, Cos(2 N_r \, \theta) + C_3 \, Cos(3 N_r \, \theta) + C_4 \, Cos(4 N_r \, \theta) \tag{5.2}$$

5.1.1 Different Modeling Methods

To determine the coefficients of the Fourier series terms, three different methods have been used:

1) Comparison Method

2) Least Square Method

3) Lagrandge Multiplier Method

1) Comparison Method: In this method, coefficients are calculated by comparing the values of capacitance obtained from FEA $\hat{C}(\theta)$, with the values obtained from equation (5.2) $C(\theta)$, at five different rotor positions i.e. at,

1) $\theta_1 = 0$ (Unaligned position)

2) $\theta_2 = \pi / N_r$ (Aligned position)

3) $\theta_3 = \pi / 2N_r$

4) $\theta_4 = \pi / 4N_r$

5) $\theta_5 = 3\pi / 4N_r$

By comparison, five set of equations are obtained as follows:

$$C_0 + C_1\, Cos(N_r\, \theta_1) + C_2\, Cos(2N_r\, \theta_1) + C_3\, Cos(3N_r\, \theta_1) + C_4\, Cos(4N_r\, \theta_1) = \hat{C}(\theta_1) \quad (5.3)$$

$$C_0 + C_1\, Cos(N_r\, \theta_2) + C_2\, Cos(2N_r\, \theta_2) + C_3\, Cos(3N_r\, \theta_2) + C_4\, Cos(4N_r\, \theta_2) = \hat{C}(\theta_2) \quad (5.4)$$

$$C_0 + C_1\, Cos(N_r\, \theta_3) + C_2\, Cos(2N_r\, \theta_3) + C_3\, Cos(3N_r\, \theta_3) + C_4\, Cos(4N_r\, \theta_3) = \hat{C}(\theta_3) \quad (5.5)$$

$$C_0 + C_1\, Cos(N_r\, \theta_4) + C_2\, Cos(2N_r\, \theta_4) + C_3\, Cos(3N_r\, \theta_4) + C_4\, Cos(4N_r\, \theta_4) = \hat{C}(\theta_4) \quad (5.6)$$

$$C_0 + C_1\, Cos(N_r\, \theta_6) + C_2\, Cos(2N_r\, \theta_6) + C_3\, Cos(3N_r\, \theta_6) + C_4\, Cos(4N_r\, \theta_6) = \hat{C}(\theta_5) \quad (5.7)$$

Equations (5.3) to (5.7) can be written in the matrix form as shown below,

$$\begin{bmatrix} 1 & Cos\theta_1 & Cos2\theta_1 & Cos3\theta_1 & Cos4\theta_1 \\ 1 & Cos\theta_2 & Cos2\theta_2 & Cos3\theta_2 & Cos4\theta_2 \\ 1 & Cos\theta_3 & Cos2\theta_3 & Cos3\theta_3 & Cos4\theta_3 \\ 1 & Cos\theta_4 & Cos2\theta_4 & Cos3\theta_4 & Cos4\theta_4 \\ 1 & Cos\theta_5 & Cos2\theta_5 & Cos3\theta_5 & Cos4\theta_5 \end{bmatrix} \begin{bmatrix} C_0 \\ C_1 \\ C_2 \\ C_3 \\ C_4 \end{bmatrix} = \begin{bmatrix} C(\theta_1) \\ C(\theta_2) \\ C(\theta_3) \\ C(\theta_4) \\ C(\theta_5) \end{bmatrix} \quad (5.8)$$

In the end equation (5.8) is solved in MATLAB to obtain the values of the coefficients of Fourier series terms.

2) Least Square Method: In this method, to calculate the coefficients of Fourier series terms, the square of error between phase capacitance value form FEA and from equation (5.2) is minimized.

Consider the error function,

$$E = \sum_{k=1}^{13} \left(C(\theta_k) - \hat{C}(\theta_k) \right)^2 \quad (5.9)$$

Where,

$$C(\theta_k) = C_0 + C_1 Cos(N_r \theta_k) + C_2 Cos(2N_r \theta_k) + C_3 Cos(3N_r \theta_k) + C_4 Cos(4N_r \theta_k)$$

$$\hat{C}(\theta_k) = Capaci\tan ce\ obtained\ \ from\ FEA$$

k represents 13 different rotor positions between aligned and unaligned positions including the aligned and unaligned positions.

Take derivative of equation (5.9) with respect to the coefficients of Fourier series terms i.e. C_0, C_1, C_2, C_3, C_4, to minimize the error as follows:

$$\frac{\partial E}{\partial C_0} = \sum_{k=1}^{13} \begin{pmatrix} C_0 + C_1 Cos(N_r \theta_k) + C_2 Cos(2 N_r \theta_k) + C_3 Cos(3 N_r \theta_k) \\ + C_4 Cos(4 N_r \theta_k) - C(\hat{\theta}_k) \end{pmatrix}$$

$$\frac{\partial E}{\partial C_1} = \sum_{k=1}^{13} Cos(\theta_k) \begin{pmatrix} C_0 + C_1 Cos(N_r \theta_k) + C_2 Cos(2 N_r \theta_k) + C_3 Cos(3 N_r \theta_k) \\ + C_4 Cos(4 N_r \theta_k) - C(\hat{\theta}_k) \end{pmatrix}$$

$$\frac{\partial E}{\partial C_2} = \sum_{k=1}^{13} Cos(2\theta_k) \begin{pmatrix} C_0 + C_1 Cos(N_r \theta_k) + C_2 Cos(2 N_r \theta_k) + C_3 Cos(3 N_r \theta_k) \\ + C_4 Cos(4 N_r \theta_k) - C(\hat{\theta}_k) \end{pmatrix}$$

$$\frac{\partial E}{\partial C_3} = \sum_{k=1}^{13} Cos(3\theta_k) \begin{pmatrix} C_0 + C_1 Cos(N_r \theta_k) + C_2 Cos(2 N_r \theta_k) + C_3 Cos(3 N_r \theta_k) \\ + C_4 Cos(4 N_r \theta_k) - C(\hat{\theta}_k) \end{pmatrix}$$

$$\frac{\partial E}{\partial C_4} = \sum_{k=1}^{13} Cos(4\theta_k) \begin{pmatrix} C_0 + C_1 Cos(N_r \theta_k) + C_2 Cos(2 N_r \theta_k) + C_3 Cos(3 N_r \theta_k) \\ + C_4 Cos(4 N_r \theta_k) - C(\hat{\theta}_k) \end{pmatrix}$$

By equating $\frac{\partial E}{\partial C_0}, \frac{\partial E}{\partial C_1}, \frac{\partial E}{\partial C_2}, \frac{\partial E}{\partial C_3}, \frac{\partial E}{\partial C_4}$ to zero, five sets of equations are obtained, which can be written in the matrix form as shown below,

$$A = \begin{bmatrix} \sum_{k=1}^{13} 1 & \sum_{k=1}^{13} Cos\theta_k & \sum_{k=1}^{13} Cos2\theta_k & ..... & \sum_{k=1}^{13} Cos4\theta_k \\ \sum_{k=1}^{13} Cos(\theta_k) & \sum_{k=1}^{13} (Cos\theta_k)^2 & \sum_{k=1}^{13} Cos2\theta_k Cos\theta_k & ..... & \sum_{k=1}^{13} Cos4\theta_k Cos\theta_k \\ \sum_{k=1}^{13} Cos(2\theta_k) & \sum_{k=1}^{13} Cos\theta_k Cos2\theta_k & \sum_{k=1}^{13} (Cos2\theta_k)^2 & ..... & \sum_{k=1}^{13} Cos4\theta_k Cos2\theta_k \\ \sum_{k=1}^{13} Cos(3\theta_k) & \sum_{k=1}^{13} Cos\theta_k Cos3\theta_k & \sum_{k=1}^{13} Cos2\theta_k Cos3\theta_k & ..... & \sum_{k=1}^{13} Cos4\theta_k Cos3\theta_k \\ 1 & & & & \\ \sum_{k=1}^{13} Cos(4\theta_k) & \sum_{k=1}^{13} Cos\theta_k Cos4\theta_k & \sum_{k=1}^{13} Cos2\theta_k Cos4\theta_k & ..... & \sum_{k=1}^{13} (Cos4\theta_k)^2 \end{bmatrix}$$

$$B = \begin{bmatrix} C_0 \\ C_1 \\ C_2 \\ C_3 \\ C_4 \end{bmatrix} \qquad C = \begin{bmatrix} \sum_{k=1}^{13} C(\hat{\theta}_k) \\ \sum_{k=1}^{13} C(\hat{\theta}_k) Cos(\theta_k) \\ \sum_{k=1}^{13} C(\hat{\theta}_k) Cos(2\theta_k) \\ \sum_{k=1}^{13} C(\hat{\theta}_k) Cos(3\theta_k) \\ \sum_{k=1}^{13} C(\hat{\theta}_k) Cos(4\theta_k) \end{bmatrix}$$

$$A\,B = C \qquad (5.10)$$

Then, equation (5.10) is solved in MATLAB to obtain the values of the coefficients of Fourier series terms.

3) Lagrandge Multiplier Method: This method is same as that of least square method. The difference is that, the error between the derivatives of capacitance form FEA and from Fourier series is also compared in this method.

So, the error function in this method is,

$$E = \sum_{k=1}^{13} \lambda_1 \left(C(\theta_k) - \hat{C}(\theta_k) \right)^2 + \lambda_2 \left(C(\theta_k)' - \hat{C}(\theta_k)' \right)^2 \qquad (5.11)$$

Where,

$C(\theta_k) = C_0 + C_1 \, Cos(N_r \, \theta_k) + C_2 \, Cos(2 N_r \, \theta_k) + C_3 \, Cos(3 N_r \, \theta_k) + C_4 \, Cos(4 N_r \, \theta_k)$

$\hat{C}(\theta_k) =$ *Capacitance obtained from FEA*

$C(\theta_k)' =$ *derivative of capacitance* $C(\theta_k)$

$\hat{C}(\theta_k)' =$ *derivative of capacitance* $\hat{C}(\theta_k)$

λ_1 *and* λ_2 *are Lagrange Multipliers*

k represents 13 different rotor positions between aligned and unaligned positions including the aligned and unaligned positions.

Take derivative of equation (5.11) with respect to the coefficients of Fourier series terms i.e. C_0, C_1, C_2, C_3, C_4, to minimize the error as follows:

$$\frac{\partial E}{\partial C_0} = \sum_{k=1}^{13} \lambda_1 \left(C_0 + C_1 Cos\left(N_r \theta_k\right) + C_2 Cos\left(2 N_r \theta_k\right) + C_3 Cos\left(3 N_r \theta_k\right) + C_4 Cos\left(4 N_r \theta_k\right) - \hat{C(\theta_k)} \right)$$

$$\frac{\partial E}{\partial C_1} = \sum_{k=1}^{13} \left[\begin{array}{l} \lambda_1 Cos(\theta_k) \left(C_0 + C_1 Cos\left(N_r \theta_k\right) + C_2 Cos\left(2 N_r \theta_k\right) + C_3 Cos\left(3 N_r \theta_k\right) + C_4 Cos\left(4 N_r \theta_k\right) - \hat{C(\theta_k)} \right) \\ + \lambda_2 \, Sin(\theta_k) \left(C_1 Sin\left(N_r \theta_k\right) + C_2 Sin\left(2 N_r \theta_k\right) + C_3 Sin\left(3 N_r \theta_k\right) + C_4 Sin\left(4 N_r \theta_k\right) + \hat{C(\theta_k)}' \right) \end{array} \right]$$

$$\frac{\partial E}{\partial C_2} = \sum_{k=1}^{13} \left[\begin{array}{l} \lambda_1 Cos(2\theta_k) \left(C_0 + C_1 Cos\left(N_r \theta_k\right) + C_2 Cos\left(2 N_r \theta_k\right) + C_3 Cos\left(3 N_r \theta_k\right) + C_4 Cos\left(4 N_r \theta_k\right) - \hat{C(\theta_k)} \right) \\ + \lambda_2 \, 2 \, Sin(2\theta_k) \left(C_1 Sin\left(N_r \theta_k\right) + C_2 Sin\left(2 N_r \theta_k\right) + C_3 Sin\left(3 N_r \theta_k\right) + C_4 Sin\left(4 N_r \theta_k\right) + \hat{C(\theta_k)}' \right) \end{array} \right]$$

$$\frac{\partial E}{\partial C_3} = \sum_{k=1}^{13} \left[\begin{array}{l} \lambda_1 Cos(3\theta_k) \left(C_0 + C_1 Cos\left(N_r \theta_k\right) + C_2 Cos\left(2 N_r \theta_k\right) + C_3 Cos\left(3 N_r \theta_k\right) + C_4 Cos\left(4 N_r \theta_k\right) - \hat{C(\theta_k)} \right) \\ + \lambda_2 \, 3 \, Sin(3\theta_k) \left(C_1 Sin\left(N_r \theta_k\right) + C_2 Sin\left(2 N_r \theta_k\right) + C_3 Sin\left(3 N_r \theta_k\right) + C_4 Sin\left(4 N_r \theta_k\right) + \hat{C(\theta_k)}' \right) \end{array} \right]$$

$$\frac{\partial E}{\partial C_4} = \sum_{k=1}^{13} \left[\begin{array}{l} \lambda_1 Cos(4\theta_k) \left(C_0 + C_1 Cos\left(N_r \theta_k\right) + C_2 Cos\left(2 N_r \theta_k\right) + C_3 Cos\left(3 N_r \theta_k\right) + C_4 Cos\left(4 N_r \theta_k\right) - \hat{C(\theta_k)} \right) \\ + \lambda_2 \, 4 \, Sin(4\theta_k) \left(C_1 Sin\left(N_r \theta_k\right) + C_2 Sin\left(2 N_r \theta_k\right) + C_3 Sin\left(3 N_r \theta_k\right) + C_4 Sin\left(4 N_r \theta_k\right) + \hat{C(\theta_k)}' \right) \end{array} \right]$$

By equating $\frac{\partial E}{\partial C_0}, \frac{\partial E}{\partial C_1}, \frac{\partial E}{\partial C_2}, \frac{\partial E}{\partial C_3}, \frac{\partial E}{\partial C_4}$ to zero, five sets of equations are obtained, which can be written in the matrix form as shown below,

$$A=\begin{bmatrix}
\sum_{k=1}^{13}\lambda_1 & \sum_{k=1}^{13}\lambda_1 Cos\theta_k & \sum_{k=1}^{13}\lambda_1 Cos2\theta_k & . & \ldots\ldots\ldots & \sum_{k=1}^{13}\lambda_1 Cos4\theta_k \\
\sum_{k=1}^{13}\lambda_1 Cos(\theta_k) & \sum_{k=1}^{13}\begin{bmatrix}\lambda_1 (Cos\theta_k)^2 + \\ \lambda_2 (Sin\theta_k)^2\end{bmatrix} & \sum_{k=1}^{13}\begin{bmatrix}\lambda_1 Cos2\theta_k Cos\theta_k + \\ \lambda_2\ 2\ Sin2\theta_k Sin\theta_k\end{bmatrix} & \ldots\ldots\ldots & & \sum_{k=1}^{13}\begin{bmatrix}\lambda_1 Cos4\theta_k Cos\theta_k + \\ \lambda_2\ 4\ Sin4\theta_k Sin\theta_k\end{bmatrix} \\
\sum_{k=1}^{13}\lambda_1 Cos(2\theta_k) & \sum_{k=1}^{13}\begin{bmatrix}\lambda_1 Cos\theta_k Cos2\theta_k + \\ \lambda_2\ 2\ Sin\theta_k Sin2\theta_k\end{bmatrix} & \sum_{k=1}^{13}\begin{bmatrix}\lambda_1 (Cos2\theta_k)^2 + \\ 4\lambda_2 (Sin2\theta_k)^2\end{bmatrix} & \ldots\ldots\ldots\ldots & & \sum_{k=1}^{13}\begin{bmatrix}\lambda_1 Cos4\theta_k Cos2\theta_k + \\ \lambda_2\ 8\ Sin4\theta_k Sin2\theta_k\end{bmatrix} \\
\sum_{k=1}^{13}\lambda_1 Cos(3\theta_k) & \sum_{k=1}^{13}\begin{bmatrix}\lambda_1 Cos\theta_k Cos3\theta_k + \\ \lambda_2\ 3\ Sin\theta_k Sin3\theta_k\end{bmatrix} & \sum_{k=1}^{13}\begin{bmatrix}\lambda_1 Cos2\theta_k Cos3\theta_k + \\ \lambda_2\ 6\ Sin2\theta_k Sin3\theta_k\end{bmatrix} & \ldots\ldots & & \sum_{k=1}^{13}\begin{bmatrix}\lambda_1 Cos4\theta_k Cos3\theta_k + \\ \lambda_2\ 12\ Sin4\theta_k Sin3\theta_k\end{bmatrix} \\
1 & & & & & \\
\sum_{k=1}^{13}\lambda_1 Cos(4\theta_k) & \sum_{k=1}^{13}\begin{bmatrix}\lambda_1 Cos\theta_k Cos4\theta_k + \\ \lambda_2\ 4\ Sin\theta_k Sin4\theta_k\end{bmatrix} & \sum_{k=1}^{13}\begin{bmatrix}\lambda_1 Cos2\theta_k Cos4\theta_k + \\ \lambda_2\ 8\ Sin2\theta_k Sin4\theta_k\end{bmatrix} & \ldots\ldots\ldots & & \sum_{k=1}^{13}\begin{bmatrix}\lambda_1 (Cos4\theta_k)^2 + \\ 16\lambda_2 (Sin4\theta_k)^2\end{bmatrix}
\end{bmatrix}$$

$$B=\begin{bmatrix}C_0\\ C_1\\ C_2\\ C_3\\ C_4\end{bmatrix} \qquad C=\begin{bmatrix}
\sum_{k=1}^{13} C(\hat{\theta}_k) \\
\sum_{k=1}^{13}\begin{bmatrix}\lambda_1\ \hat{C}(\theta_k) Cos\theta_k - \\ \lambda_2\ \hat{C}(\theta_k)' Sin\theta_k\end{bmatrix} \\
\sum_{k=1}^{13}\begin{bmatrix}\lambda_1\ \hat{C}(\theta_k) Cos2\theta_k - \\ \lambda_2\ 2\ \hat{C}(\theta_k)' Sin2\theta_k\end{bmatrix} \\
\sum_{k=1}^{13}\begin{bmatrix}\lambda_1\ \hat{C}(\theta_k) Cos3\theta_k - \\ \lambda_2\ 3\ \hat{C}(\theta_k)' Sin3\theta_k\end{bmatrix} \\
\sum_{k=1}^{13}\begin{bmatrix}\lambda_1\ \hat{C}(\theta_k) Cos4\theta_k - \\ \lambda_2\ 4\ \hat{C}(\theta_k)' Sin4\theta_k\end{bmatrix}
\end{bmatrix}$$

$$A\,B = C \qquad (5.12)$$

Then, equation (5.12) is solved in MATLAB to obtain the values of the coefficients of Fourier series terms.

5.1.2 Simulation Results

The capacitance data from FEA that is used in all the three methods is given in table 5.1 below.

Table 5.1 Capacitance Data from FEA

Position of Rotor (Degrees)	Capacitance Value (F/m)	Derivative of Capacitance
0	5.01 e-11	0
2.5	5.10 e-11	2.12e-11
5	5.48 e-11	8.70e-11
7.5	6.67 e-11	2.74e-10
10	1.02 e-10	7.97e-10
12.5	1.32 e-10	8.43e-10
15	1.75 e-10	8.49e-10
17.5	2.12 e-10	8.44e-10
20	2.49 e-10	8.44e-10
22.5	2.86e-10	8.37e-10
25	3.22e-10	8.26e-10
27.5	3.56e-10	7.81e-10
30	3.74e-10	4.21e-10

1) Comparison Method: This method uses five different values of capacitances from FEA, at five different rotor positions viz. 0, 7.5, 15, 22.5 and 30 degrees given in table 5.1, and compares it with the values obtained from equation (5.2) at same rotor positions, as explained above. The Fourier series coefficients thus obtained by solving matrix equation (5.8) in MATLAB are C_0 = 0.1849e-9, C_1 = -0.1585e-9, C_2 = 0.0185e-9, C_3 = -0.0034e-9, C_4 = 0.0086e-9.

2) Least Square Method: In this method, equation (5.9) uses all 13 values of capacitances given in table 5.1, as obtained from FEA. Matrix equation (5.10) is then solved in MATLAB to get values of coefficients of Fourier series terms as C_0 = 0.1855e-9, C_1 = -0.1562e-9, C_2 = 0.0168e-9, C_3 = -0.0041e-9, C_4 = 0.0084e-9.

3) Lagrandge Multiplier Method: This method uses values of capacitances as well as derivative of capacitances given in table 5.1, as obtained from FEA, in equation (5.11). Equation (5.12) is then solved in MATLAB to get values of coefficients of Fourier series terms as C_0 = 0.1854e-9, C_1 = -0.1568e-9, C_2 = 0.0171e-9, C_3 = -0.0041e-9, C_4 = 0.0089e-9.

Thus, a unique Fourier series is generated from all the three methods for the phase capacitance of the micro VCM.

Figure 5.1 compares the capacitances obtained from FEA and from three different modeling methods, explained above.

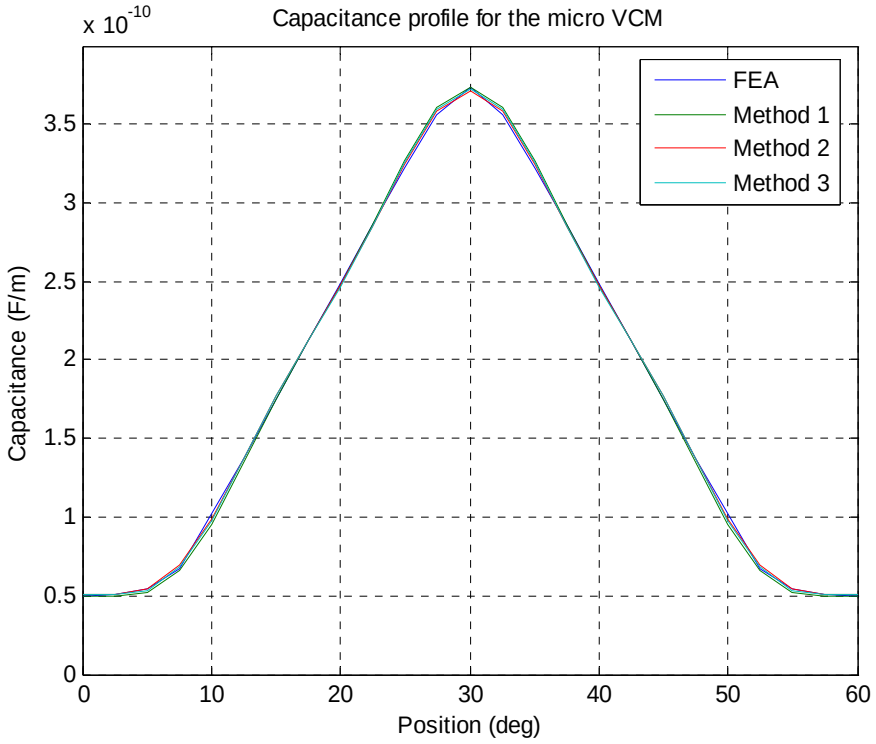

Figure 5.1 Capacitance profile as obtained from FEA and the three modeling methods

Now, since from equation (3.3)

$$T = \frac{1}{2} V^2 \frac{dC}{d\theta}$$

From equation (5.2)

$$C(\theta) = C_0 + C_1 Cos(N_r \theta) + C_2 Cos(2 N_r \theta) + C_3 Cos(3 N_r \theta) + C_4 Cos(4 N_r \theta) \quad (5.13)$$

Thus,

$$T(\theta) = -N_r \left(C_1 Sin(N_r \theta) + 2 C_2 Sin(2 N_r \theta) + 3 C_3 Sin(3 N_r \theta) + 4 C_4 Sin(4 N_r \theta)\right) \quad (5.14)$$

Figure 5.2 compares the torque profile as obtained from FEA and the three modeling methods.

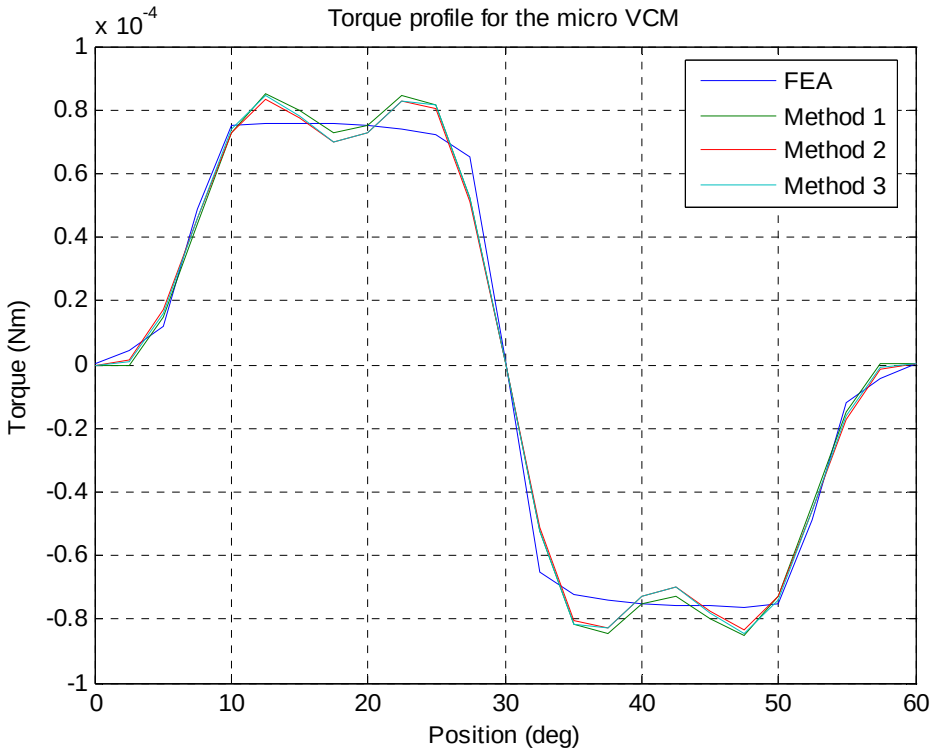

Figure 5.2 Torque profile as obtained from FEA and the three modeling methods

Thus, the profiles obtained form three different modeling techniques almost match with the profiles obtained from FEA. However, first modeling method i.e. method of comparison is considered the best as the profiles obtained from this method are closest to the profiles obtained from FEA. Also, it requires minimum data from FEA i.e. only 5 points as opposite to 13 points in the other two methods.

CHAPTER 6

DYNAMIC MODELING AND TORQUE/VOLT MAXIMIZATION

6.1 Dynamic Model

In this section, dynamic model of the micro VCM along with its drive electronics has been developed using Simulink. This model is then used to maximize the toque/volt performance of the machine by optimizing the conduction angles of switches in the power electronics circuit, used to drive the micro VCM.

The dynamic model of the micro VCM is based upon the following equations [12]:

From equation (3.8),

$$i = \frac{v}{r} + C(\theta_r)\frac{dv}{dt} + v\,\frac{dC(\theta_r)}{dt}$$

Neglecting the resistance of the machine, we get

$$C(\theta_r)\frac{dv}{dt} = i - v\,\frac{dC(\theta_r)}{dt} \tag{6.1}$$

$$\frac{dv}{dt} = \left(i - v\omega\,\frac{dC(\theta_r)}{d\theta} \right) / C(\theta_r) \tag{6.2}$$

From equation (3.3)

$$T = \frac{1}{2} V^2\,\frac{dC}{d\theta}$$

From equation (5.2)

$$C(\theta) = C_0 + C_1\,Cos(N_r\,\theta) + C_2\,Cos(2N_r\,\theta) + C_3\,Cos(3N_r\,\theta) + C_4\,Cos(4N_r\,\theta)$$

Where, C_0 = 0.1849e-9, C_1 = -0.1585e-9, C_2 = 0.0185e-9, C_3 = -0.0034e-9, C_4 = 0.0086e-9. Equation (6.2) is then implemented in the Simulink model of micro VCM to find the phase voltage v, where i is the DC link current, $C(\theta_r)$ is the phase capacitance and ω is the angular speed of the rotor (in radians per second). At each step of simulation, phase voltage is calculated depending upon the value of ω, $C(\theta_r)$, $\frac{dC(\theta_r)}{d\theta}$ and i. This voltage is then used to calculate torque using equation (3.3). In this way, all the four phases are implemented in the Simulink model. Figure 6.1 shows the dynamic model of micro VCM along with its drive electronics.

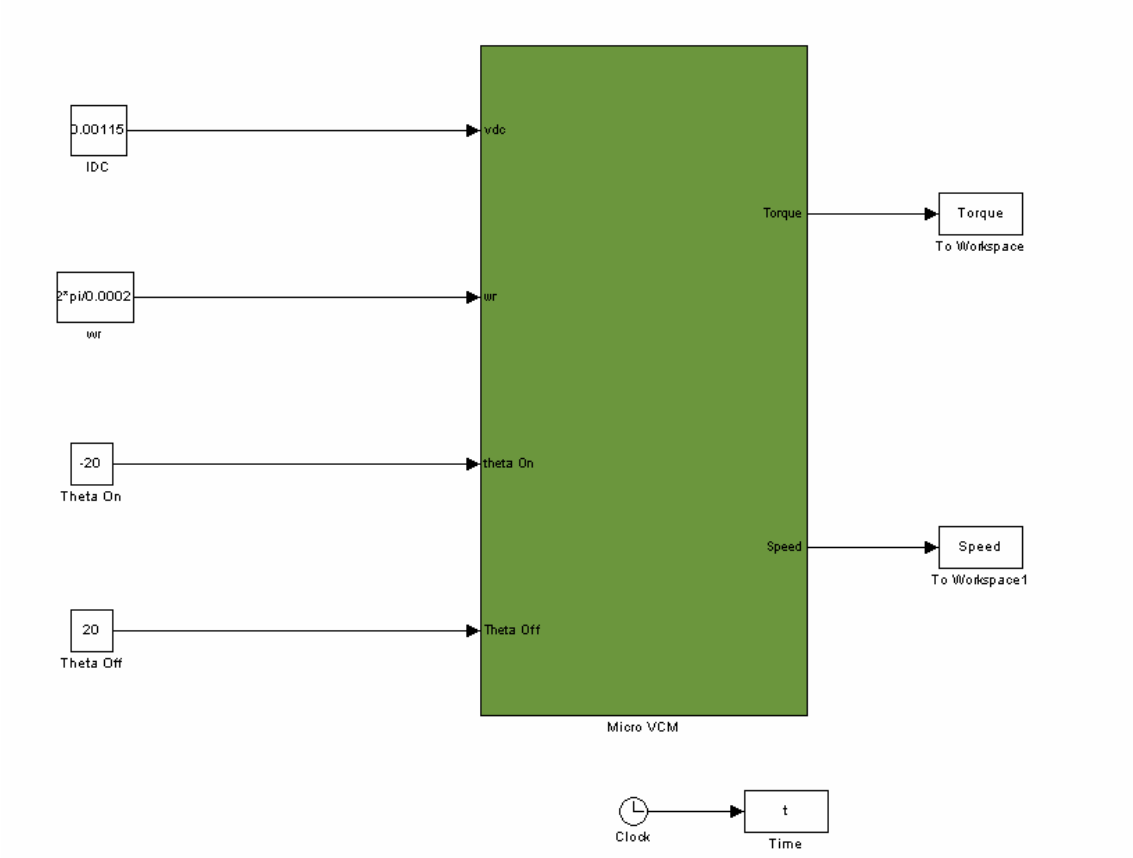

Figure 6.1 Dynamic model of micro VCM

The input to micro VCM are the input current, turn on and turn off angles of the switches. The output parameters are Torque and Speed of the micro VCM Torque is the overall produced torque, which is the sum of the torques from all the four phases. Speed of the machines is in radians per second. The micro VCM block contains,

1) **Drive Electronics** to drive each phase of the machine, i.e. a number of switches to give pulses of current to the machine for excitation. Figure 6.2 shows the inside of the micro VCM block.

2) **Capacitance Calculation Block** for each phase of the machine to calculate capacitance at each simulation step as described above.

3) **Dynamic Equations and Torque Calculation Block** for each phase of the machine which calculates phase voltage for the machine at each simulation step and consequently the torque is calculated as described above.

4) **Total Torque Calculation Block** adds up the torque of each phase and gives the overall produced torque of VCM.

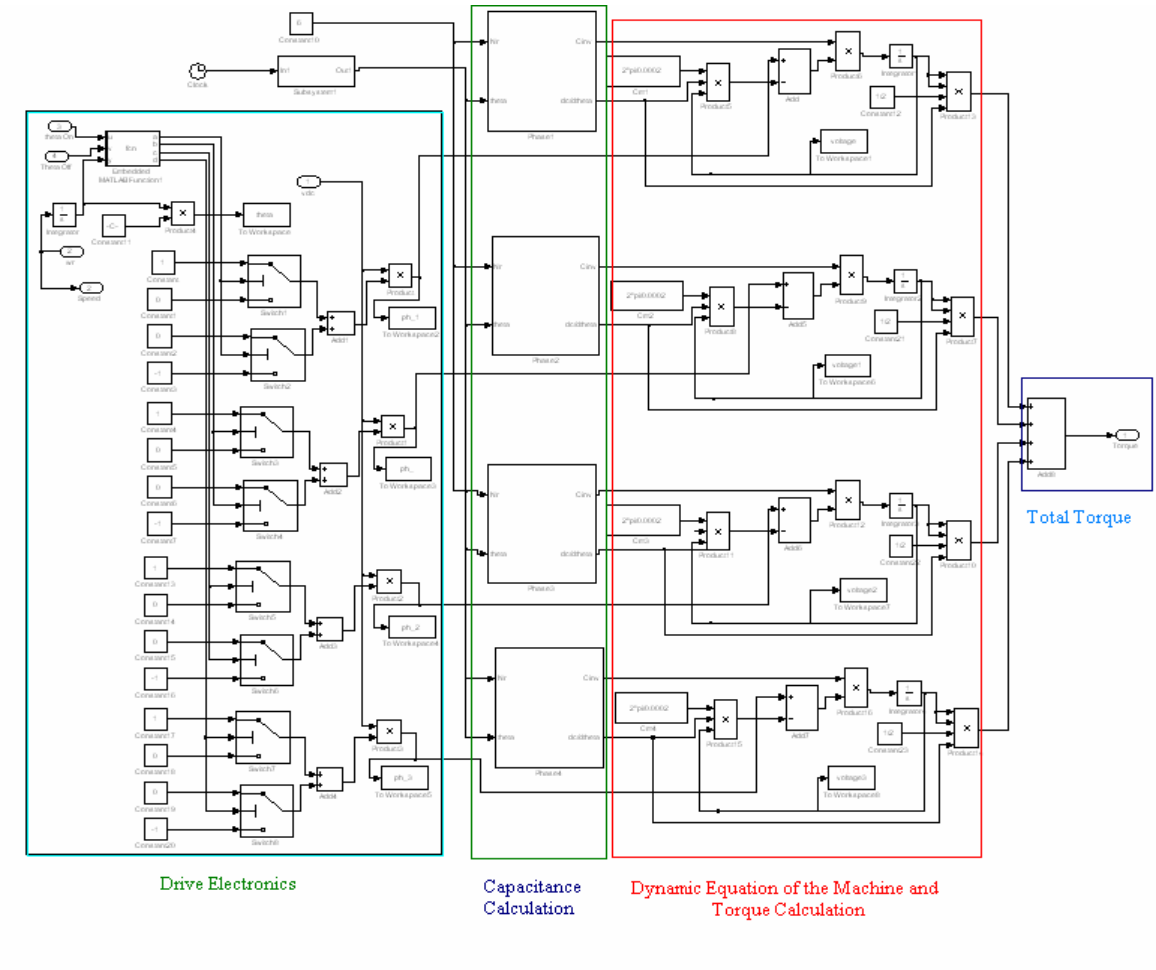

Figure 6.2 Inside of the micro VCM

Initially the machine is operated at speed of 20,000 rpm. The input current source has a value of 0.00115 A, which is sufficient to maintain a phase voltage of 300 Volts across the stator electrodes and rotor. Zero degree is the unaligned position of the machine.

The drive electronics use 2 switches for each phase to generate the positive and negative pulses of current for each phase of the machine over a cycle of 60 degrees. The duration of the positive pulse is also called the conduction angle. The turn on and turn

off angle decide the duration of the positive pulse and negative pulses applied to the machine. At turn on angle, the switch operates in a manner to generate positive pulse of current and phase current of 0.00115 A is applied to phase A of the machine. At turn off angle, the positive pulse ends, and a negative pulse of current is applied to the same phase. The duration of negative pulse is equal to the positive pulse duration. For remaining time i.e. 60 degrees minus the positive and negative pulse duration, the current applied to phase A is zero. The pulses applied to phase B, C and D are shifted by 15, 30 and 45 degrees respectively. Thus, for a turn on and turn off angle of 0 and 20 degrees respectively, the current pulses generated for phase A, B , C and D of the machine over a period of 180 electrical degrees are shown in figures 6.3, 6.4, 6.5, 6.6 respectively.

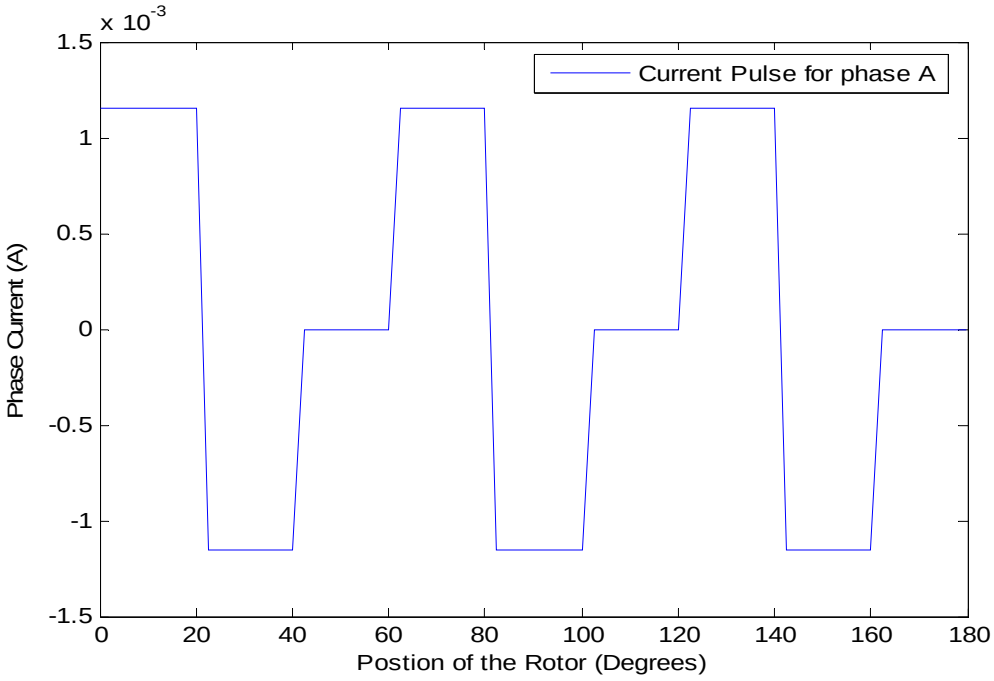

Figure 6.3 Current pulses for phase A

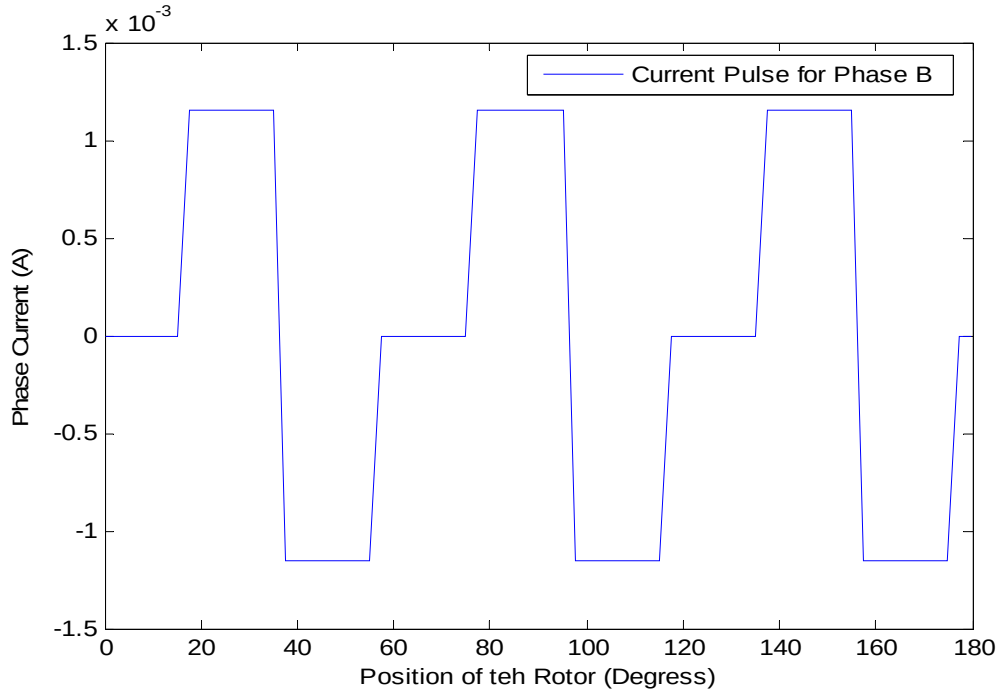

Figure 6.4 Current pulses for phase B

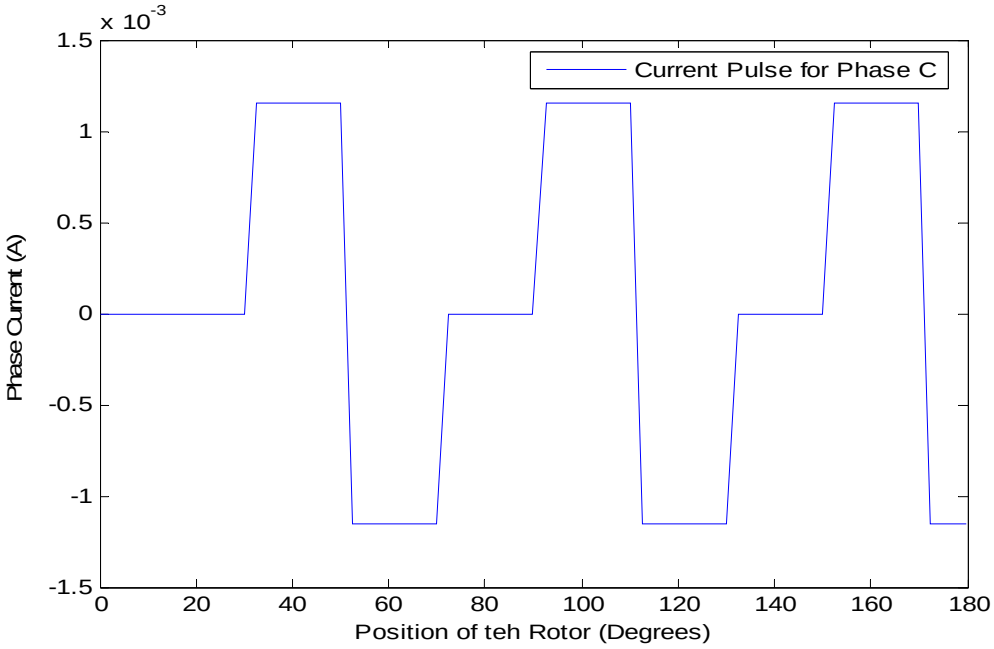

Figure 6.5 Current pulses for phase C

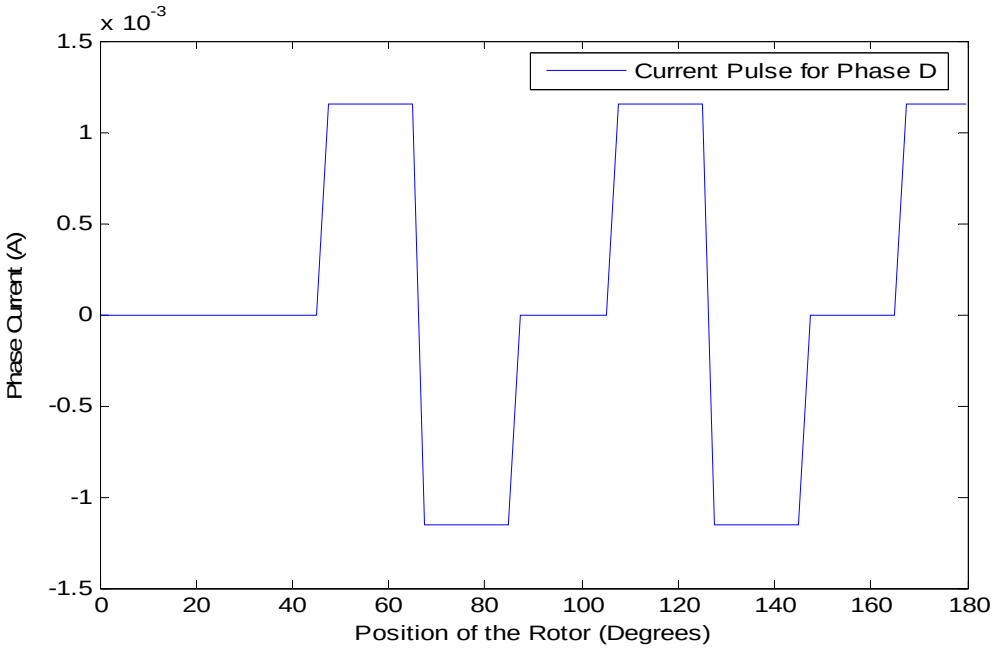

Figure 6.6 Current pulses for phase D

In the capacitance calculation block at each simulation step i.e. for each new value of θ, Capacitance is calculated based upon the Fourier series generated for the capacitance of the micro VCM using the comparison method in the last chapter. Also, $\frac{dC}{d\theta}$ is calculated for same value of θ, for each phase of the machine.

In the dynamic equation and torque calculation block, the dynamic equation (6.2) and torque equation (3.3), are implemented using integration, addition and multiplication blocks. At each simulation step new value of phase voltage is calculated which is used along with θ and $\frac{dC}{d\theta}$ calculated above to give a value for the torque generated by a single phase of the machine.

Using the Addition block in total torque calculation block, torque generated from each phase is summed up and the value of total torque produced by the micro VCM is calculated.

6.2 Torque/Volt Maximization by Conduction Angle Optimization

This section describes the Torque/Volt maximization of the micro VCM by optimizing the turn on and turns off angles of the switches. At a speed of 20,000 rpm the input current source of 0.00115 A has been chosen to maintain a phase voltage of 300 Volts. As the speed of the machine increases, the dependent current load draws more and more current (from equation (6.2)).

$$\frac{dv}{dt} = \left(i - v\omega \frac{dC(\theta_r)}{d\theta} \right) / C(\theta_r)$$

Since, dependent current load opposes the DC link current, it becomes difficult to maintain a phase voltage of 300 Volts across the stator and rotor. Thus, torque of the machine decreases consequently. This section aims at maximizing the torque/volt capability of the machine by optimizing the turn on, and turn off, angles of the drive electronics.

As the speed of the machine increases, the turn off angles is advanced by a few degrees i.e. the current source is switched off a few degrees before the aligned position of the machine. In this way, machine does not cross the aligned position, thereby producing a negative torque.

Now, the average torque/volt values (over the same time period) for a single phase of the machine, operating at speeds ranging from 20,000 rpm to 50,000 rpm, have

been compared for different combinations of turn and turn off angles. Then, the optimum combination of turn and turn off angles, for which the machine has maximum average torque/volt value, is obtained at one particular operating speed. In this way, the aim of torque maximization is achieved by conduction angle optimization. The unaligned and aligned positions of the machine are 0 and 30 degrees respectively. While maximizing the torque, it should be noticed that phase voltage of the machine should not exceed 300 Volts.

1) At operating speed of 20,000 rpm

Table 6.1 Average Torque/Volt Values for Different Turn on and Turn off Angles

Turn On and Turn Off Angles (Degrees)	Average Torque/Volt (Nm/V)	Turn On and Turn Off Angles (Degrees)	Average Torque/Volt (Nm/V)
(-3,17)	2.67e-4	(-4,11)	4.13e-8
(-3,20)	2.44e-4	(-4,16)	4.64e-8
(-3,22)	2.25e-4	(-4, 19)	4.55e-8
(-3,27)	2.71e-4	(-4,21)	4.31e-8

For angle advancement above 4 degrees, phase voltage exceeds the limit of 300 volts. Thus, maximum torque/volt value is obtained at conduction angle of (-4, 16).

2) At operating speed of 25,000 rpm

Table 6.2 Average Torque/Volt Values for Different Turn on and Turn off Angles

Turn On and Turn Off Angles (Degrees)	Average Torque/Volt (Nm/V)	Turn On and Turn Off Angles (Degrees)	Average Torque/Volt (Nm/V)
(-6,12)	3.62e-8	(-7,11)	3.56e-8
(-6,14)	3.80e-8	(-7,13)	3.80e-8
(-6,17)	3.86e-8	(-7,16)	3.92e-8
(-6,19)	3.76e-8	(-7,18)	3.88e-8

For angle advancement above 7 degrees, phase voltage exceeds the limit of 300 volts. Thus, maximum torque/volt value is obtained at conduction angle of (-7, 16).

3) At operating speed of 30,000 rpm

Table 6.3 Average Torque/Volt Values for Different Turn on and Turn off Angles

Turn On and Turn Off Angles (Degrees)	Average Torque/Volt (Nm/V)	Turn On and Turn Off Angles (Degrees)	Average Torque/Volt (Nm/V)
(-9,11)	3.04e-8	(-10,13)	3.27e-8
(-9,14)	3.28e-8	(-10,15)	3.34e-8
(-9,16)	3.32e-8	(-10,18)	3.28e-8
(-9,21)	2.95e-8	(-10,20)	3.10e-8

For angle advancement above 10 degrees, phase voltage exceeds the limit of 300 volts. Thus, maximum torque/volt value is obtained at conduction angle of (-10, 15).

4) At operating speed of 35,000 rpm

Table 6.4 Average Torque/Volt Values for Different Turn on and Turn off Angles

Turn On and Turn Off Angles (Degrees)	Average Torque/Volt (Nm/V)	Turn On and Turn Off Angles (Degrees)	Average Torque/Volt (Nm/V)
(-11,12)	2.74e-8	(-12,11)	2.67e-8
(-11,14)	2.84e-8	(-12,13)	2.82e-8
(-11,17)	2.83e-8	(-12,16)	2.87e-8
(-11,19)	2.72e-8	(-12,18)	2.79e-8

For angle advancement above 12 degrees, phase voltage exceeds the limit of 300 volts. Thus, maximum torque/volt value is obtained at conduction angle of (-12, 16).

5) At operating speed of 40,000 rpm

Table 6.5 Average Torque/Volt Values for Different Turn on and Turn off Angles

Turn On and Turn Off Angles (Degrees)	Average Torque/Volt (Nm/V)	Turn On and Turn Off Angles (Degrees)	Average Torque/Volt (Nm/V)
(-14,9)	2.18e-8	(-15,7)	1.80e-8
(-14,11)	2.42e-8	(-15,10)	2.33e-8
(-14,14)	2.57e-8	(-15,13)	2.55e-8
(-14,16)	2.57e-8	(-15,15)	2.58e-8

For angle advancement above 15 degrees, phase voltage exceeds the limit of 300 volts. Thus, maximum torque/volt value is obtained at conduction angle of (-15, 15).

6) At operating speed of 45,000 rpm

Table 6.6 Average Torque/Volt Values for Different Turn on and Turn off Angles

Turn On and Turn Off Angles (Degrees)	Average Torque/Volt (Nm/V)	Turn On and Turn Off Angles (Degrees)	Average Torque/Volt (Nm/V)
(-16,7)	1.60e-8	(-17,8)	1.80e-8
(-16,9)	1.94e-8	(-17,11)	2.15e-8
(-16,12)	2.21e-8	(-17,13)	2.25e-8
(-16,14)	2.27e-8		

For angle advancement above 17 degrees, phase voltage exceeds the limit of 300 volts. Thus, maximum torque/volt value is obtained at conduction angle of (-16, 14).

7) At operating speed of 50,000 rpm

Table 6.7 Average Torque/Volt Values for Different Turn on and Turn off Angles

Turn On and Turn Off Angles (Degrees)	Average Torque/Volt (Nm/V)	Turn On and Turn Off Angles (Degrees)	Average Torque/Volt (Nm/V)
(-19,6)	1.29e-8	(-20,5)	1.08e-8
(-19,9)	1.78e-8	(-20,8)	1.65e-8
(-19,11)	1.96e-8	(-20,10)	1.89e-8

For angle advancement above 20 degrees, phase voltage exceeds the limit of 300 volts. Thus, maximum torque/volt value is obtained at conduction angle of (-19, 11).

Summarizing the results obtained above, a look up table for optimum conduction angles to obtain maximum torque/volt for the single phase of the micro VCM operating at speeds, ranging from 20,000 rpm to 50,000 rpm, has been obtained.

Table 6.8 Look–up Table

Operating Speed (rpm)	Optimum Conduction Angles (Degrees)	Operating Speed (rpm)	Optimum Conduction Angles (Degrees)
20,000	(-4,16)	40,000	(-15,15)
25,000	(-7,16)	45,000	(-16,14)
30,000	(-10,15)	50,000	(-19,11)
35,000	(-12,16)		

Figure 6.7 compares the torque plots of phase A of the micro VCM, operating at speeds varying from 20,000 rpm to 50,000 rpm, at optimum conduction angles.

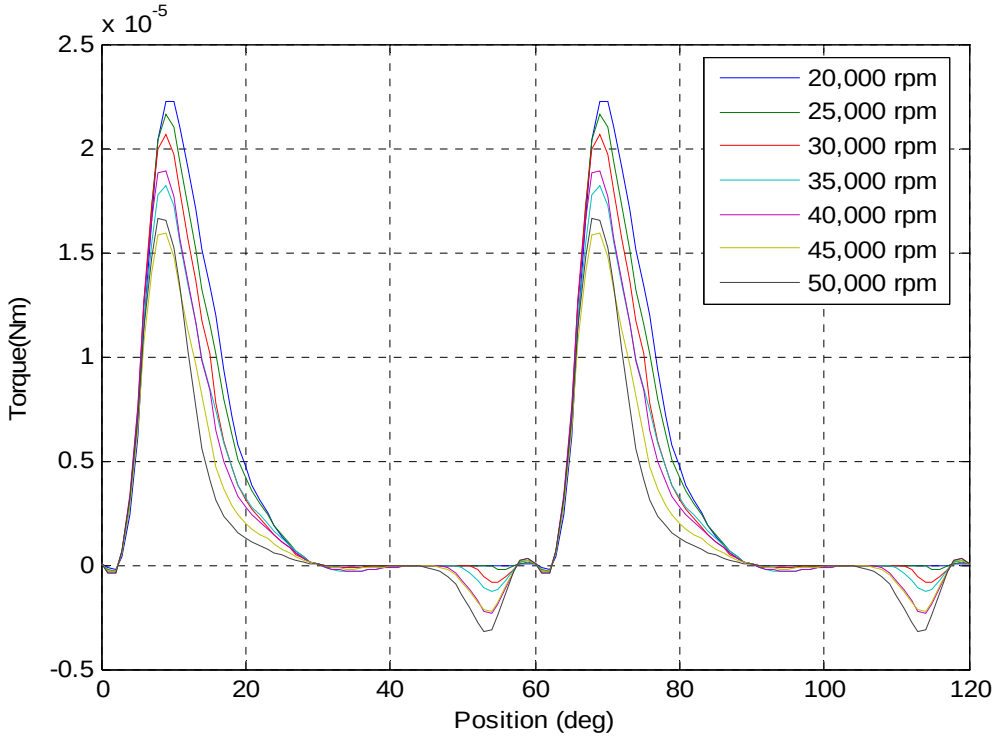

Figure 6.7 Torque plots of micro VCM for phase A

It is evident from the figure 6.7 that as the speed of the machine increases, torque decreases, for a constant DC link current value, as explained above.

Figure 6.8 shows the phase voltage plots of the micro VCM, operating at speeds varying from 20,000 rpm to 50,000 rpm, at optimum conduction angles.

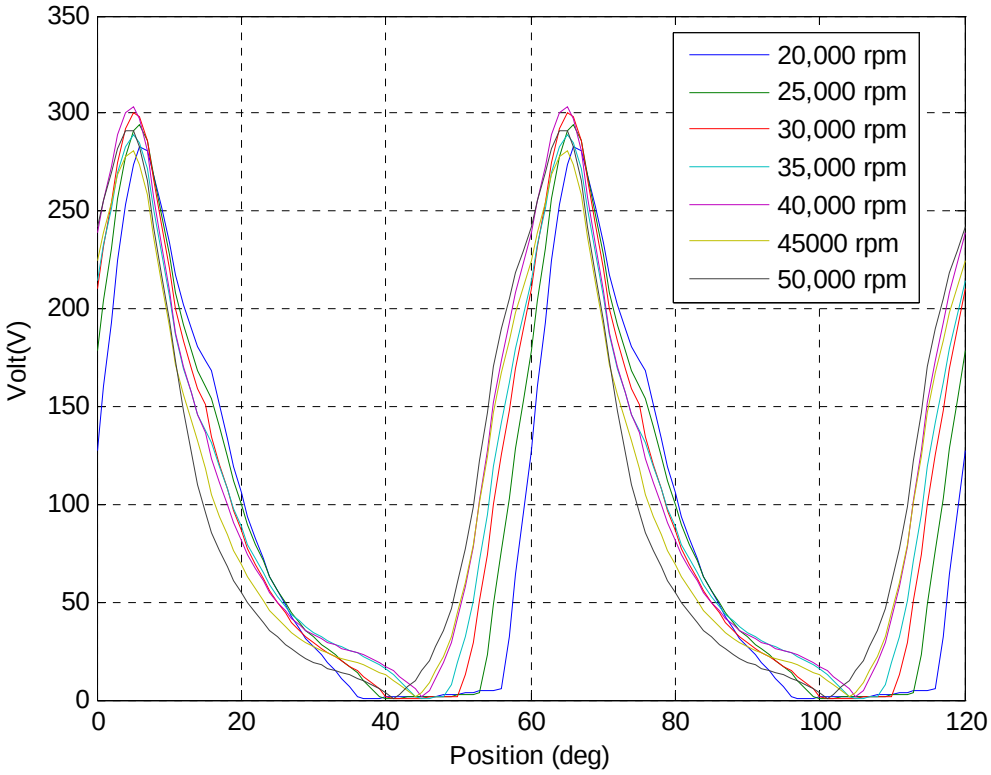

Figure 6.8 Phase voltage plot of micro VCM for phase A

It is evident from the figure 6.8 that effective phase voltage rises as the positive pulse of current is applied to a particular phase as according to equation (6.2). As the current becomes negative, the voltage starts decreasing; there is a forced decay in the voltage and as the current becomes zero, the voltage drops naturally, involving two different time constants thereby.

CHAPTER 7

CONCLUSIONS

A two dimensional finite element model of an 8/6 four phase micro variable capacitance machine (VCM) has been developed using Maxwell Electrostatic solver. The procedure for selecting the rotor and stator arc length has been described. The effects of machine geometry, such as stator, rotor arc lengths and air gap length, on capacitance and torque profile of the machine has been studied in detail. The tangential and normal components of the electrostatic forces, in the air gap of the machine, have been investigated to study the effect of mutual fluxes in micro VCM. Also, modeling of the phase capacitance has been done using three different methods and then these methods are compared to get most accurate Fourier series expression for the phase capacitance. Then, the dynamic model of the micro VCM has been developed using Simulink, to maximize the toque/volt performance of the machine by conduction angle optimization.

APPENDIX A

DATA OF THE MICRO VCM

Stator poles: 8

Rotor Poles: 6

Number of Phases: 4

Excitation Voltage: 300 Volts

Mechanical Speed: 50,000 rpm

Electrical Frequency of Excitation: 5000 Hz

Stator Electrodes Outer Radius: 0.45mm

Stator Electrodes Inner Radius: 0.3mm

Rotor Outer Radius: 0.297mm

Rotor Inner Radius: 0.147mm

Stator Arc Length: 21˚

Rotor Arc Length: 23˚

Air-gap Length: 0.003mm

REFERENCES

1) Krause P.C., Wasynczuk O., Sudhoff S. D., Analysis of Electric Machines, IEEE Press, 1996

2) Maluf N., An Introduction to Microelectromechanical Systems, Artech House, 2000.

3) Agrawal R., Hasan Q., Ashraf N., Sundaram K. B., “Design and Fabrication of Meso-Scale Variable Capacitance Motor for Miniature Heat Pumps”, Journal of Micromechanics and Microengineering, vol.13, no. 1, Jan. 2003, p. 1-7. Journal Paper

4) Chapman P. L., Krein, P. T., “Micro-motor technology: electric drive designer's perspective”, IEEE, 2001, p. 1978-83, vol.3. Conference Paper

5) Chapman P. L., “Efficiency Issues in Variable –Capacitance Micromotor Drives”, IEMDC Conference, 2005. Invitation Paper.

6) Salman A., Napieralski A., Jablonski G., “Simulation and Optimization of Variable Capacitance (VC) Micromotors, using Modified Parallel- Plate Model”, Technical Proceedings of the International Conference on Modeling and Simulation of Microsystems, 1999, pg 609-612.

7) Liu Chang-Tsung, Chiang Tsung-Shiun, “On the Magnetic Saturation of a Micro Linear Switched Reluctance Motor”, IEEE Transactions on Magnetics, volume 40, Issue 4, Part 2, July 2004, pg 2861-2863.

8) Fujita H., “Microactuators and Micromachines”, Proceedings of the IEEE, vol. 86, Issue 8, Aug. 1998, pg 1721-1732.

9) Irudayaraj Sujay S., Emadi A., “Micromachines: Principles of Operation, Dynamics and Control”, IEMDC Conference, 2005. Invitation Paper.

10) Bart S. F., Lang J. H., “Electroquasistatic Induction Micromotors”, Micro Electro Mechanical Systems, 1989, Proceedings, ‘An Investigation of Micro Structures, Sensors, Actuators, Machines and Robots’, IEEE 20-22 Feb 1989, pg 7-12

11) Hameyer K., Johansson T. B., “Finite Element Simulations for the Design of Micro Electromechanical Systems”, presented at IEE Seminar on Current Trends in the Use of Finite Elements in Electromechanical Design and Analysis, London, January 2000.

12) Krishnamurthy M., Jindal A., Fahimi B., “Operational Characteristics of Variable Capacitance Micromotor Drives: A Preliminary Investigation”, IEMDC Conference 2005. Invitation Paper.

13) Vijayraghavan P., Design of Switched Reluctance Motors and Development of a Universal Controller for Switched Reluctance and Permanent Magnet Brushless DC Motor Drives, Dissertation, Nov. 2001.

14) Akyuz M., Berg M., Larsson A., Thottappillil R., “Calculation of the Electrostatic Force Acting on Axisymmetric Objects in Non – Uniform Electric Fields”, IEE Conference Publication, v 2, n 467, 1999, p 2.71.P6-2.74.P6.

15) Mahdavi J., Suresh G., Fahimi B., Ehsani M., “Dynamic Modeling of Non-Linear SRM Drive with PSpice”, Conference Record - IAS Annual Meeting (IEEE Industry Applications Society), v 1, 1997, p 661-667.

BIOGRAPHICAL INFORMATION

Amita Jindal was born in Ludhiana, India in 1981. She completed her undergraduate studies at Thapar Institute of Engineering and Technology, India and received her B. E. degree in Electrical Engineering in May 2003. She started her graduate studies at University of Missouri-Rolla in January 2004. She then took a transfer to University of Texas at Arlington in August 2004 and is currently pursuing her Masters degree in Electrical Engineering. She has been working as a Graduate Research Assistant in Power Electronics and Controlled Motion Lab since 2004. Her current research interests are in the areas of Micro Machines and Power Electronics.